Climate Sensitivity is Sensitive to Changes in Ocean Heat Transport

Hansi Singh,[a] Nicole Feldl,[b] Jennifer E. Kay,[c] and Ariel L. Morrison[a]

[a] University of Victoria, Victoria, British Columbia, Canada
[b] University of California, Santa Cruz, Santa Cruz, California
[c] University of Colorado Boulder, Boulder, Colorado

ABSTRACT: Do changes in ocean heat transport (OHT) that occur with CO_2 forcing, impact climate sensitivity in Earth system models? Changes in OHT with warming are ubiquitous in model experiments: when forced with CO_2, such models exhibit declining poleward OHT in both hemispheres at most latitudes, which can persist over multicentennial time scales. To understand how changes in OHT may impact how the climate system responds to CO_2 forcing, particularly climate sensitivity, we perform a series of Earth system model experiments in which we systematically perturb OHT (in a slab ocean, relative to its preindustrial control climatology) while simultaneously doubling atmospheric CO_2. We find that equilibrium climate sensitivity varies substantially with OHT. Specifically, there is a 0.6 K decrease in global mean surface warming for every 10% decline in poleward OHT. Radiative feedbacks from CO_2 doubling, and the warming attributable to each of them, generally become more positive (or less negative) when poleward OHT increases. Water vapor feedback differences account for approximately half the spread in climate sensitivity between experiments, while differences in the lapse rate and surface albedo feedbacks account for the rest. Prescribed changes in OHT instigate opposing changes in atmospheric energy transport and the general circulation, which explain differences in atmospheric water vapor and lapse rate between experiments. Our results show that changes in OHT modify atmospheric radiative feedbacks at all latitudes, thereby driving changes in equilibrium climate sensitivity. More broadly, they demonstrate that radiative feedbacks are not independent of the coupled (atmosphere and ocean) dynamic responses that accompany greenhouse gas forcing.

KEYWORDS: Atmosphere; Ocean; Atmosphere-ocean interaction; Energy transport; Feedback; Forcing; Climate change; Climate sensitivity; Climate variability; General circulation models

1. Introduction

Climate sensitivity, the global-mean temperature response of the Earth system to CO_2 doubling, is one of the fundamental quantities of interest in Earth system science (Hansen et al. 1984; Knutti and Hegerl 2008). Both the magnitude of global warming and its pace have major implications for societal mitigation, adaptation, and resilience (Orlove 2005; Mertz et al. 2009; Barnett et al. 2015; LoPresti et al. 2015). While climate science has advanced in leaps and bounds over the last 50 years, climate sensitivity continues to be a quantity that is difficult to constrain. The latest estimates of equilibrium climate sensitivity fall in the range of 1.5–4.5 K, a spread that has remained largely unchanged over the past several decades (Charney et al. 1979; Knutti et al. 2017; Sherwood et al. 2020). At least some of this range may be irreducible (see, e.g., Roe and Baker 2007).

The ocean is one of many factors that influence how the climate system responds to CO_2 forcing. The enormous heat capacity of the ocean makes it the primary heat reservoir of the climate system. Over decadal to multidecadal to centennial time scales, the rate at which the ocean takes up heat determines the pace of transient climate change (Raper et al. 2002; Sokolov et al. 2003; Stouffer et al. 2006). While the

upper ocean can absorb heat from above at all latitudes, it is only over the subpolar oceans that surface heat can penetrate into the deep ocean, either through mixing by eddies on surface-outcropping isopycnal surfaces (as in the Southern Ocean; see Morrison et al. 2016) or through deep convection (as occurs over Antarctic coastal regions or in the Nordic seas; see, e.g., Bitz et al. 2006). In comparisons of climate models, those that have stronger subpolar ocean heat uptake generally experience weaker transient warming, while the reverse is true for those with weaker subpolar ocean heat uptake (Raper et al. 2002; Boé et al. 2009).

A variety of factors impact the rate of heat uptake into the deep ocean, including surface winds (particularly over the Southern Ocean; see, e.g., Russell et al. 2006) and ocean stratification at sites of deep convection (Kuhlbrodt and Gregory 2012). Evidence also suggests that active ocean processes, including redistribution of ocean temperature through circulation changes, help control ocean heat uptake and thereby set the pace of transient climate change (Banks and Gregory 2006; Xie and Vallis 2012). This redistribution of ocean heat content has the most pronounced effects in the North Atlantic, where it triggers more negative (i.e., stabilizing) radiative feedbacks that moderate surface warming (Rugenstein et al. 2016; Trossman et al. 2016; Garuba et al. 2017).

Given that the ocean helps set the pace of transient climate change, an interesting follow-up question is this: besides ocean heat uptake, does the ocean impact either equilibrium or transient warming through other mechanisms, such as heat

---

ⱺ Denotes content that is immediately available upon publication as open access.

transport? Several studies indicate that poleward ocean heat transport warms the Earth system (Rind and Chandler 1991; Winton 2003; Herweijer et al. 2005; Rencurrel and Rose 2018), suggesting that any changes in ocean heat transport concomitant with CO_2 forcing might impact just how much the Earth system warms. Indeed, this sensitivity to changing poleward ocean heat transport is evident in the Arctic: greater poleward ocean heat transport into the Arctic with CO_2 forcing is associated with greater sea ice loss, more surface warming, and stronger polar amplification (Holland and Bitz 2003; Mahlstein and Knutti 2011; Hwang et al. 2011; Singh et al. 2017). Other studies suggest that the magnitude of weakening in the Atlantic meridional overturning circulation, which decreases northward ocean heat transport over the Atlantic basin, determines the magnitude of surface warming in the Northern Hemisphere (Rugenstein et al. 2013; Lin et al. 2019; Weijer et al. 2020; Liu et al. 2020).

Despite the above, there is also evidence suggesting that changes in ocean heat transport over long time scales are small, and therefore do not impact surface warming significantly. A standard approach for estimating equilibrium climate sensitivity is to assess surface warming following CO_2 doubling in a global climate model (GCM) utilizing a slab ocean, in which the ocean heat flux convergence in the mixed layer is specified to be that of a fully dynamic ocean from a preindustrial run (see the pioneering study of Wilson and Mitchell 1987). The major assumption underlying such an approach is that the ocean heat transport does not change with CO_2 forcing. Danabasoglu and Gent (2009) showed that this assumption of unchanged ocean heat transport with CO_2 doubling was not unreasonable, at least in a single model: a fully coupled GCM, integrated to equilibrium following CO_2 doubling, had global mean warming very similar to that of the same GCM with a slab ocean. Furthermore, Danabasoglu and Gent (2009) found that changes in ocean heat transport in the fully coupled experiment were generally small over such long time scales, justifying the assumption that equilibrium warming can be approximated by assuming that ocean heat transport does not change.

While the results of Danabasoglu and Gent (2009) are compelling, their study used a single GCM, the T31 × 3 CCSM3, which was state-of-the-art at the time, but is low resolution and not fully comprehensive by today's modeling standards. Furthermore, Li et al. (2013) performed a similar study utilizing a model of a similar generation, ECHAM3, and found much larger changes in ocean heat transport that persisted to equilibrium. As such, it is possible that the minimal ocean heat transport changes identified in CCSM3 by Danabasoglu and Gent (2009) are not a common feature of most GCMs. Furthermore, while both Li et al. (2013) and Danabasoglu and Gent (2009) found that the equilibrium climate sensitivity was similar between the slab ocean and fully coupled experiments, both identified substantial regional differences in warming between the two experiments, suggesting that changes in ocean heat transport in the fully coupled run were impacting the climate system response to forcing. Indeed, Danabasoglu and Gent (2009) caution that a slab ocean model should only be used to estimate equilibrium climate sensitivity if changes in ocean heat transport at equilibrium are small.

Here, we revisit and expand upon the studies of Danabasoglu and Gent (2009) and Li et al. (2013), to better understand *how* changes in ocean heat transport impact the way the climate system responds to CO_2 forcing. The major question we seek to answer is this: if ocean heat transport were to change with CO_2 doubling, and such changes persisted over long time scales, would the climate sensitivity change? And if so, through what mechanisms do changes in ocean heat transport affect the climate sensitivity, both globally and regionally? To answer these questions, we first examine how CO_2 forcing instigates changes in ocean heat transport and surface temperature in a collection of state-of-the-art models participating in the phase 6 of the Climate Model Intercomparison Project (CMIP6). We next assess how ocean heat transport and surface temperatures evolve over multi-centennial time scales, following abrupt CO_2 doubling, in the fully coupled Community Earth System Model, version 1 (CESM1). We then use a version of CESM1 (coupled to a slab ocean rather than a dynamic one) to model how idealized, prescribed changes in ocean heat transport, which occur concurrently with CO_2 doubling, impact the climate system's forced response. We analyze these through the complementary lenses of radiative feedbacks and energetics, to understand exactly how changes in ocean heat transport impact the way the climate system responds to CO_2 forcing. Notably, we find that changing ocean heat transport impacts equilibrium climate sensitivity through its effects on atmospheric energy transport and radiative feedbacks. We finish by discussing important implications of our work for studies of climate sensitivity and the many factors likely underlying it.

2. Methods

a. Analysis of CMIP6 models

We assessed ocean heat transport and transient warming in a collection of Earth system models participating in the sixth phase of the Climate Model Intercomparison Project (CMIP6). We analyzed climatologies of the final 30 years (years 2070–2100) of the SSP585 experiment (high emissions scenario, with a radiative forcing of 8.5 W m^{-2} by 2100; see O'Neill et al. 2016), and the final 50 years (years 100–150) of the Abrupt4XCO2 experiment (abrupt CO_2 quadrupling at year 1; see Eyring et al. 2016). For each model, we compared these to that model's piControl, an equilibrated 1850s preindustrial control experiment (Eyring et al. 2016). For our analysis, we used all models with data archived on the Lawrence Livermore Earth System Grid Federation node, for which necessary output variables were available.

For each model, we approximated the ocean heat transport (OHT) at latitude ϕ as an integral of the zonal mean surface fluxes R_{sfc} from the south pole to latitude ϕ (Peixoto and Oort 1992):

$$\text{OHT} = 2\pi r_E^2 \int_0^\phi (R_{sfc} - \overline{R_{sfc}})\cos\phi \, d\phi, \qquad (1)$$

where r_E is the radius of Earth, $\overline{R_{sfc}}$ is the net ocean heat uptake (calculated as the area-weighted mean of the surface fluxes), and R_{sfc} includes radiative and turbulent contributions. We note that the above equation is exact for an equilibrated experiment (such as piControl), but less exact when there are inhomogeneous changes in ocean heat storage, as in the SSP585 and Abrupt4XCO2 experiments (Peixoto and Oort 1992; He et al. 2019).

b. CESM1 fully coupled and slab ocean model experiments

We used the state-of-the-art Community Earth System Model, version 1 (CESM1; Hurrell et al. 2013) to explore relationships between poleward OHT changes and surface warming with CO_2 doubling. CESM1 includes version 5 of the Community Atmosphere Model (CAM5; Neale et al. 2012), version 4 of the Community Land Model (CLM4; Oleson et al. 2010), and version 4 of the Community Sea Ice Code (CICE4; Hunke and Lipscomb 2010). The fully coupled CESM1 utilizes version 2 of the Parallel Ocean Program (POP2; Danabasoglu et al. 2012), while the CESM1 coupled to a slab ocean (hereafter CESM1-SOM) is formulated using "q-fluxes," prescribed ocean heat flux convergence in the climatological mixed layer (either derived from an equilibrated, fully coupled preindustrial run, or constructed otherwise; see formulation of the SOM in Bitz et al. 2012). All model components are at a nominal horizontal resolution of 1°.

To understand how the fully coupled Earth system (including ocean heat transport and surface temperature) responds to CO_2 forcing over multi-centennial time scales, we performed a fully coupled CO_2-doubling experiment with CESM1. We branched this experiment from year 1000 of the CESM1 Large Ensemble preindustrial control (CESM1-LE; Kay et al. 2015), and kept all model components and constituents configured identically to those in the preindustrial CESM1-LE. At the start of the experiment, we doubled atmospheric CO_2 abruptly relative to its preindustrial concentration (from 284.7 to 569.4 ppm), and integrated forward in time for 850 years. For assessing changes in ocean heat transport with time in CESM1, we used the POP2 model variable NHEAT, which records the exact OHT from on-the-fly calculations as the model integrates forward in time.

To evaluate how idealized changes in ocean heat transport impact the global climate response to CO_2 forcing, we performed five CO_2-doubling experiments with CESM1-SOM. We branched these five experiments from the end of a 60-yr preindustrial control CESM1-SOM run, which was forced with prescribed monthly climatological q-fluxes computed from those in the equilibrated, fully coupled, preindustrial CESM1-LE control run (Kay et al. 2015). We doubled CO_2 abruptly at the start of each experiment, and simultaneously adjusted the climatological q-flux to be equal to one of five constructed spatial fields (shown in Fig. 4 and described further in the accompanying text): amplified by 15% and 30% over all latitudes and seasons, relative to the climatological preindustrial q-flux, to produce the OHT + 15% and OHT + 30% CO_2-doubling experiments; diminished by 15% and 30% over all latitudes and seasons, relative to the climatological preindustrial q-flux, to produce the OHT − 15% and OHT − 30% CO_2-doubling experiments; and held equal to the climatological preindustrial q-flux, to produce the Control OHT CO_2-doubling experiment. We ran each of these CESM1-SOM runs for 60 years, and calculated climatologies from the last 30 years of each of these runs, when the experiments are in equilibrium (i.e., the global net top-of-the-atmosphere imbalance is less than 0.05 W m^{-2}). We calculated the CO_2-doubling response in each of these experiments relative to a control climatology from our (equilibrated) preindustrial CESM1-SOM run.

3. Results

a. Analysis of fully coupled models

We first examine how ocean heat transport (OHT) responds to CO_2 forcing in a collection of Earth system models participating in the 6th phase of the Climate Model Intercomparison Project (CMIP6; Fig. 1). In both the SSP585 experiments (Figs. 1a,b) and Abrupt4XCO2 experiments (Figs. 1c,d), we find that poleward OHT declines with CO_2 forcing. In the Southern Hemisphere, poleward OHT decreases by about 0.2 PW at 30°S in both SSP585 and Abrupt4XCO2; in the Northern Hemisphere, poleward OHT decreases by about 0.2 PW at 30°N in SSP585, and by nearly 0.4 PW at 30°N in Abrupt4XCO2. This decrease in poleward OHT is not only evident in both of these forced experiments, but is also ubiquitous across models (note multimodel range in OHT change denoted by cyan shading in Figs. 1b,d). We further note that the OHT response is somewhat asymmetric about the equator: poleward OHT declines more in the Northern Hemisphere than in the Southern Hemisphere, particularly in Abrupt4XCO2. This asymmetry reflects the very different hemispheric processes giving rise to this decline in poleward OHT: a slowdown of the Atlantic meridional overturning circulation, which manifests as a decline in poleward OHT in the Northern Hemisphere and a decline in northward cross-equatorial OHT (Nummelin et al. 2017; He et al. 2019); and northward transport of excess heat taken up by the Southern Ocean, which manifests as a decline in poleward OHT in the Southern Hemisphere (He et al. 2019). Moreover, the greatest spread in poleward OHT between models is found in the Northern Hemisphere between 30° and 45°N, with a range of 0.5 PW in SSP585 and a range of 0.8 PW in Abrupt4XCO2.

We next consider the relationship between surface warming and changes in poleward OHT in these CMIP6 models. Figure 2 shows the zonal surface temperature change in SSP585 (Fig. 2a) and Abrupt4XCO2 (Fig. 2c), with lines color coded by the poleward OHT change at 45°N (red lines indicate models with less than average declines in poleward OHT, and blue lines indicate models with greater than average declines in poleward OHT). In both SSP585 and Abrupt4XCO2, we find that models that warm more than average (in the Northern Hemisphere) experience weaker than average declines in poleward OHT, while models that warm less than average experience stronger declines in poleward OHT (Figs. 2a,c; note that red lines mostly lie above the
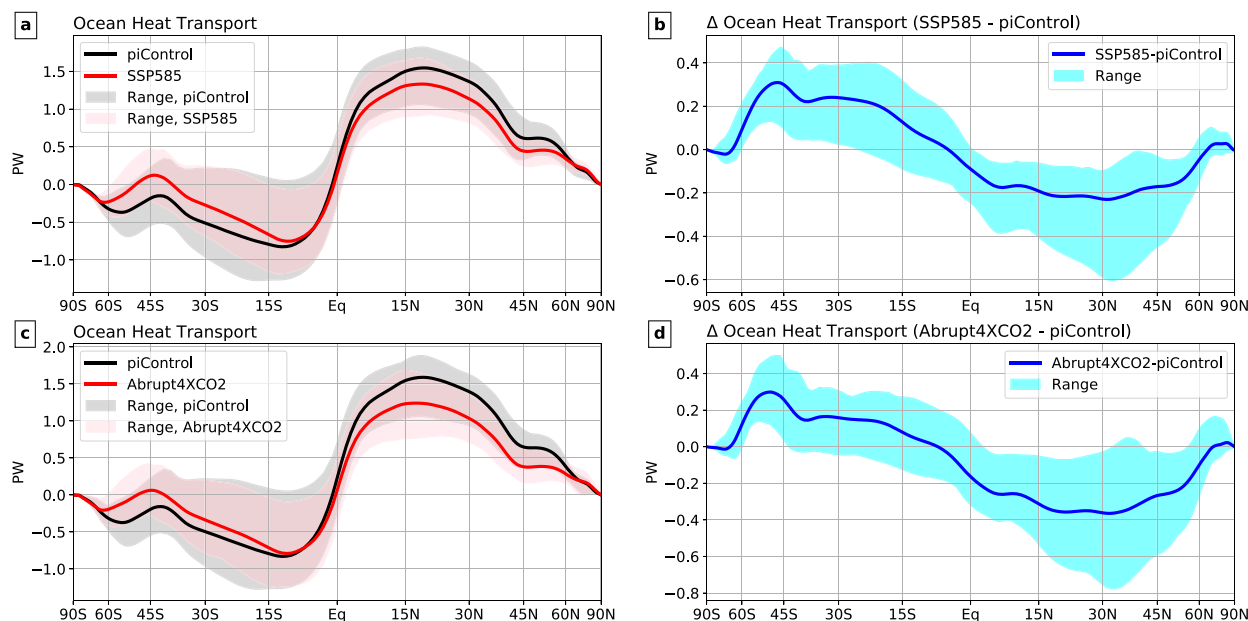
FIG. 1. Ocean heat transport in CMIP6-participating Earth system models: (a) ocean heat transport in piControl and SSP585 (years 2070–2100); (b) change in ocean heat transport in SSP585, years 2070–2100, relative to piControl; (c) ocean heat transport in piControl and Abrupt4XCO2 (years 100–150 following abrupt CO_2 quadrupling); and (d) change in ocean heat transport in Abrupt4XCO2, years 100–150, relative to piControl. Ocean heat transport is approximated using Eq. (1). In all panels, multimodel means are denoted by thick lines, and the multimodel range is indicated by the shaded envelope.

multimodel mean in the Northern Hemisphere, while blue lines lie below the multimodel mean). Indeed, the change in poleward OHT at 45°N is weakly correlated with the Northern Hemispheric mean surface warming in these experiments (Figs. 2b,d; $r = 0.5$ for SSP585 and $r = 0.4$ for Abrupt4XCO2, with $p < 0.05$ for both). This relationship is most pronounced for models with the greatest warming, which all experience only weak declines in poleward OHT at 45°N. On the other hand, models with moderate or weak warming tend to experience a greater range of OHT decline. We do not find a similar relationship in the Southern Hemisphere, possibly because other factors like clouds (see, e.g., Grise and Polvani 2014; Kay et al. 2014) and Southern Ocean heat uptake (Kuhlbrodt and Gregory 2012) are much more important for setting the pace of transient warming in this hemisphere over these time scales.

In Fig. 3, we examine the evolution of poleward OHT and surface warming following abrupt CO_2 doubling in the fully coupled CESM1. As we found in the CMIP6 multimodel archive, poleward OHT declines with CO_2 forcing in CESM1 (Fig. 3a). Notably, we find that this decrease in poleward OHT persists over at least 850 years following abrupt CO_2 doubling, suggesting that changes in OHT continue to be a feature of the climate system response to CO_2 forcing well after transient adjustments. Moreover, we find that the hemispheric decline in poleward OHT is highly correlated with surface warming in that hemisphere (Figs. 3b,c; $r = 0.7$ and $r = -0.8$ in the Northern and Southern Hemispheres, respectively, with $p < 0.05$ for both): lower hemispheric mean surface temperatures are associated with a greater decline in poleward OHT in the midlatitudes (45°N and 45°S), while

warmer temperatures are associated with a weaker decline in poleward OHT. The slope of this relationship differs between the hemispheres: the change in poleward OHT per unit change in surface temperature is twice as large in the Northern Hemisphere as in the Southern Hemisphere (0.09 versus 0.05 PW K^{-1}). We also note that these slopes are similar in magnitude to the relationships found between changes in OHT at 45°N and Northern Hemispheric warming among CMIP6 models (0.05 and 0.06 PW K^{-1} for SSP585 and Abrupt4XCO2 experiments, respectively; recall Fig. 1).

b. CO_2-doubling slab ocean model experiments

1) RESPONSE TO CO_2 DOUBLING

Our analysis of fully coupled Earth system models suggests that a decline in poleward OHT often accompanies CO_2 forcing (recall Fig. 1 and Fig. 3a), and that this decline in poleward OHT is correlated with warming (in the Northern Hemisphere in CMIP6 models, recalling Fig. 2; and in both hemispheres in the fully coupled CESM1, recalling Figs. 3b,c). However, analyses such as these do not establish a causal relationship between OHT changes and transient climate sensitivity. In such fully coupled experiments, it is unclear if changes in OHT are responsible for differences in warming between experiments, or if changes in OHT are merely a response to the magnitude of warming.

To ascertain whether changes in OHT impact climate sensitivity, we perform a series of abrupt CO_2-doubling experiments with the CESM1-SOM in which we systematically perturb the (prescribed) OHT in the slab ocean relative to
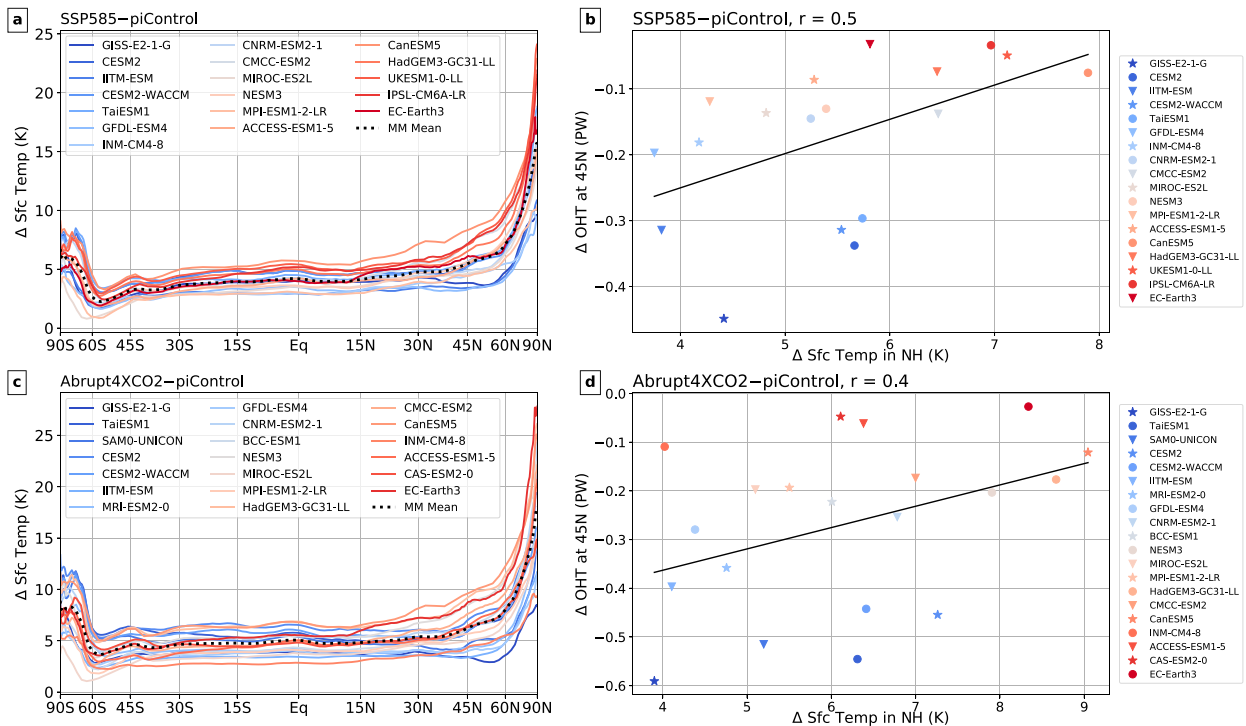
FIG. 2. Relationships between changes in ocean heat transport (OHT) and changes in surface temperature in CMIP6-participating models: (a) surface temperature change in SSP585, years 2070–2100, relative to piControl, color coded by the change in OHT at 45°N (redder colors indicate models with less decline in OHT while bluer colors indicate models with greater decline in OHT), with the multimodel mean indicated by the black dotted line; (b) Northern Hemispheric warming in SSP585, years 2070–2100, vs the change in OHT at 45°N, with the best-fit regression line shown in black; (c) as in (a), but for Abrupt4XCO2, years 100–150; and (d) as in (b), but for Abrupt4-XCO2, years 100–150.

that in the preindustrial control, to model the effect of OHT changes that might occur with CO_2 forcing. We construct the idealized OHT profiles used in these CO_2-doubling experiments by amplifying or diminishing the preindustrial control OHT by either 15% or 30% (shown in Fig. 4): OHT + 30% (dark red line), OHT + 15% (light red line), OHT − 15% (light blue line), and OHT − 30% (dark blue line). A fifth reference experiment, Control OHT (gray line), assumes that OHT remains unchanged from its preindustrial control value following CO_2 doubling. Figure 4 also shows the OHT response to CO_2 doubling in the fully coupled CESM1 (dotted green lines), which indicates that the OHT − 15% experiment most closely approximates the CO_2-forced decline in OHT in this model.

All CESM1-SOM experiments are integrated to equilibrium following CO_2 doubling, and we analyze annual climatologies over the final 30 years of these experiments. We assess the climate system response to CO_2 doubling in these experiments relative to a CESM1-SOM preindustrial control run. We describe this experimental setup in further detail in section 2b. Because each of these experiments differ only in the OHT prescribed in the slab ocean, differences in the CO_2-doubling response must result from differences in OHT.

In Fig. 5, we examine the energy transport response to CO_2 doubling in our CESM1-SOM experiments. The prescribed

OHT is as expected from the experimental setup (cf. Figs. 4–5a), with OHT + 15% and OHT + 30% experiments having greater poleward OHT relative to the preindustrial control (red-hued lines in Fig. 5a), and OHT − 15% and OHT − 30% having weaker poleward OHT (blue-hued lines in Fig. 5a). Small deviations in the energy transport in the Control OHT experiment are evident (see deviations of gray line away from x axis) and attributable to differences in sea ice growth and transport with CO_2 doubling.

In each of these experiments, the atmospheric energy transport (AET) response to CO_2 doubling opposes the prescribed OHT changes. In experiments with increasing poleward OHT, poleward AET decreases (see red-hued lines, 5b), and in experiments with decreasing poleward OHT, poleward AET increases (see blue-hued lines). Indeed, changes in AET are minimal when there are no prescribed OHT changes (see gray line), presumably because there are no OHT changes to oppose. Compensation between poleward atmosphere and ocean energy transports is unsurprising, and is ubiquitous in climate modeling studies (see, e.g., Bjerknes 1964; Vellinga and Wood 2002; Vellinga and Wu 2008; Kang et al. 2008; Farneti and Vallis 2013).

While compensation between the (prescribed) OHT and AET response is evident in our experiments, we also note that this compensation is imperfect: AET changes only oppose about two-thirds of OHT changes at most latitudes,
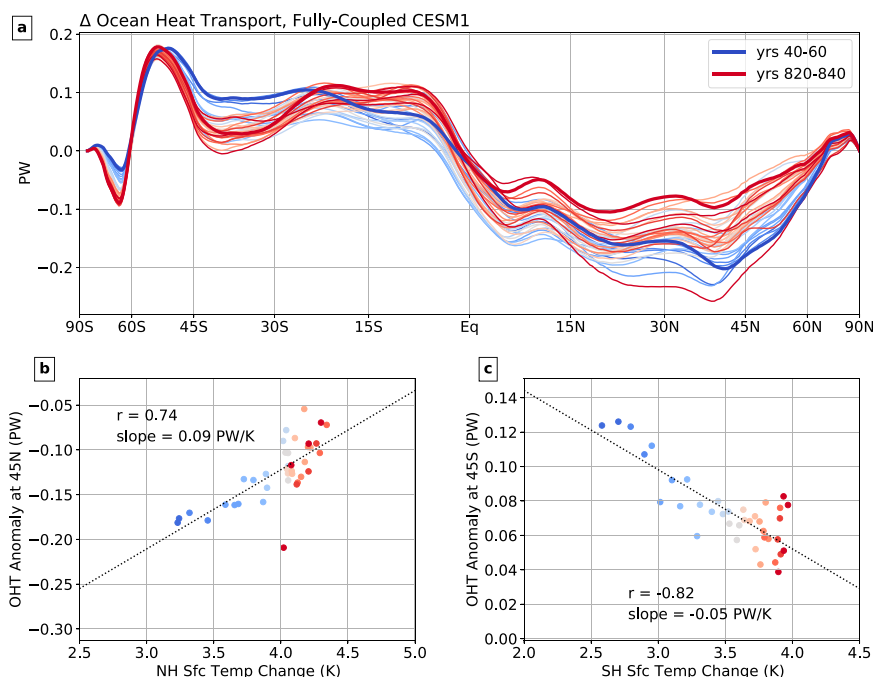
F<small>IG</small>. 3. Changes in OHT and surface temperature with abrupt CO_2 doubling in the fully coupled CESM1: (a) change in OHT (PW), calculated over consecutive, non-overlapping 20-yr intervals, starting from years 40 to 60 following abrupt CO_2 doubling (thick blue line), extending to years 820–840 (thick red line), with intermediate intervals indicated by thin lines (color coded chronologically by time interval, from blue to red); (b) relationship between Northern Hemispheric surface temperature change and the change in OHT at 45°N, over consecutive 20-yr intervals from years 40 to 840 (with points color coded chronologically by time interval, from blue to red); (c) as for (b), but for Southern Hemispheric surface temperature change and the change in OHT at 45°S. Lines of best fit are shown in (b) and (c).

which results in a total energy transport response (AET plus prescribed OHT) that is generally in the same direction as the prescribed OHT, but roughly one-third the magnitude (see Fig. 5c). That the total energy transport change is small, compared to much larger changes in OHT and AET, has been investigated extensively in prior studies (see, e.g., Stone 1978). We also observe that the total energy transport is smaller for some experiments than others: AET changes more effectively compensate for decreasing OHT (i.e., blue-hued lines in Fig. 5c lie close to 0° at latitudes south of 15°N) than for increasing OHT (i.e., the large magnitude of red-hued lines in the Northern Hemisphere in Fig. 5c).

Figures 6 and 7a show the surface temperature response to CO_2 doubling in each of the CESM1-SOM experiments. We find that warming with CO_2 doubling is greatest when poleward OHT increases (Figs. 6a,b, which show warming in the OHT + 30% and OHT + 15% experiments, respectively; also see red-hued lines in Fig. 7a) and weakest when poleward OHT decreases (Figs. 6d,e, which show warming in the OHT − 15% and OHT − 30% experiments, respectively; also see blue-hued lines in Fig. 7a). In particular, we find that warming in the OHT + 30% and OHT + 15% experiments exceeds that in Control OHT over most latitudes and regions (Figs. 6f,g), while warming in the OHT −

15% and OHT − 30% experiments is weaker than that in Control OHT nearly everywhere (Figs. 6i,j). Differences in warming are evident over nearly all latitudes, but are greatest over the mid- and high latitudes in both hemispheres. Indeed, it is only over the deep tropics (between 5°N and 5°S) where zonal mean warming is slightly greater in the experiments with decreasing poleward OHT than with increasing poleward OHT (Fig. 7a).

When we normalize the surface temperature response by the global mean surface temperature change, we find that warming is strongly polar amplified when poleward OHT increases (red-hued lines in Fig. 7b), and only weakly polar amplified when poleward OHT decreases (blue-hued lines). In OHT − 30%, where prescribed poleward OHT is 30% weaker than that in the preindustrial, warming is actually amplified toward the tropics, except at the highest latitudes (dark blue line in Fig. 7b).

In Fig. 7c, we show the global mean surface temperature change with CO_2 doubling (i.e., the equilibrium climate sensitivity) in each of our CESM1-SOM experiments as a function of the percentage change in poleward OHT relative to that in the preindustrial control. As described previously, climate sensitivity increases when poleward OHT increases (relative to that in the preindustrial control) and decreases when poleward OHT
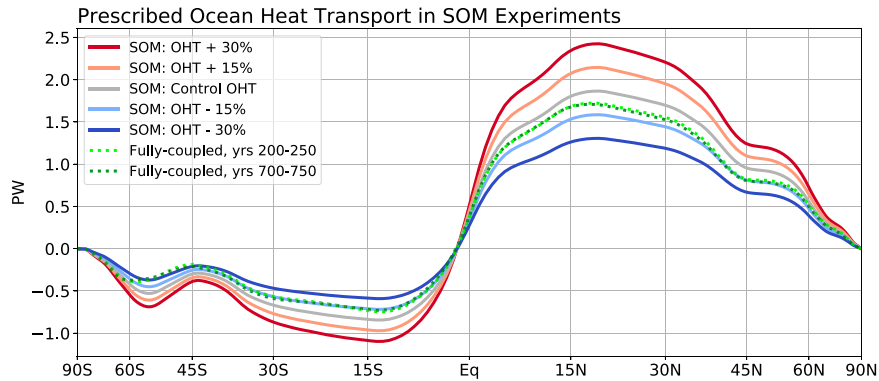
FIG. 4. Prescribed OHT in CESM1-SOM CO_2-doubling experiments (solid lines). Prescribed OHT in Control OHT (gray line) is identical to that in the fully coupled CESM1 preindustrial control experiment; OHT + 30% (dark red line) and OHT + 15% (light red line) have prescribed OHT that is 30% and 15% greater in magnitude than Control OHT, respectively; and OHT − 30% (dark blue line) and OHT − 15% (light blue line) have prescribed OHT that is 30% and 15% smaller in magnitude than Control OHT, respectively. Green dotted lines show OHT in the fully coupled CESM1 following abrupt CO_2 doubling: at years 200–250 (light green line) and years 700–750 (dark green line).

decreases. In particular, we find that a 10% change in poleward OHT changes climate sensitivity by 0.5 K, as reckoned from a simple linear regression ($r = 0.98$). We also note that how sensitive the climate sensitivity is to changes in poleward OHT depends on the direction in which it changes. Specifically, a 15% increase in poleward OHT increases climate sensitivity by only 0.5 K, but a 15% decrease in poleward OHT decreases climate sensitivity by a much larger 0.9 K. We note that the latter is comparable to the relationship between changes in poleward OHT and surface temperature with CO_2 doubling in the fully coupled CESM1 (recall Fig. 3), albeit weaker in magnitude: a 0.15 PW decline in OHT at 45°N causes 1 K less equilibrium warming in our CESM1-SOM experiments, while a smaller 0.07 PW decline in OHT at 45°N corresponds to 1 K less transient warming in the fully coupled CESM1.

As we described previously, CO_2 doubling in the fully coupled CESM1 is accompanied by a 10%–15% decline in poleward OHT at most latitudes and over a range of time scales (recall Fig. 4). Our CESM1-SOM experiments suggest that such a modest decline in poleward OHT, similar to that in the OHT − 15% experiment, results in a CO_2-doubling response with significantly less warming in the extratropics and only slightly more warming in the deep tropics, relative to the response when poleward OHT is unchanged. Therefore, a decline in poleward OHT partially counteracts warming due to CO_2 doubling itself. To understand how changes in poleward OHT impact climate sensitivity in this way, we next evaluate the climate response in the CESM1-SOM experiments using a framework of radiative feedbacks and energetics.

2) ANALYSIS OF RADIATIVE FEEDBACKS AND ENERGETICS

To assess how differences in (prescribed) poleward OHT in our experiments drive differences in the CO_2-doubling response, we begin by examining the local radiative feedbacks

(Figs. 8a–f), which we compute using the kernel method (Soden et al. 2008; Shell et al. 2008), utilizing radiative kernels derived from CAM5 (see Pendergrass et al. 2018). Feedbacks computed using relative humidity (RH) as the state variable (see Held and Shell 2012, for a description of constant RH feedbacks) are shown in Figs. 9a–c. Because all of these are local feedbacks, and are therefore normalized by the zonal-mean (not global) temperature change, they assume that the local top-of-the-atmosphere radiative flux change is proportional to local surface warming (see Feldl and Roe 2013, for a discussion of how local and global radiative feedbacks differ), which risks misattributing local and remote controls on feedbacks and may result in ill-defined feedbacks where zonal-mean warming is muted (such as over the North Atlantic or Southern Oceans in transient simulations). We note that each of the radiative feedbacks differ between experiments (Figs. 8a–e, which show the Planck, lapse rate, water vapor, cloud, and surface albedo feedbacks, respectively; also see Figs. 9a–c, which show the constant-RH Planck, constant-RH lapse rate, and RH water vapor feedbacks), and these differences lead to differences in the strength of the total feedback between experiments (Fig. 8f). Not surprisingly, the total feedback with CO_2 doubling is less negative when poleward OHT increases, and is more negative when poleward OHT decreases (cf. red-hued and blue-hued lines in Fig. 8f), consistent with greater climate sensitivity in the former than the latter.

To quantify how much each radiative feedback contributes to the surface warming in each experiment, we decompose the zonal mean energetic anomaly due to CO_2 doubling into components due to local feedbacks, forcing, and energy transports (as described in Feldl and Roe 2013). In brief, this anomaly can be written as

$$R_F(\theta) = \sum_i \lambda_i(\theta)\Delta T(\theta) - \Delta[\nabla \cdot F_{atm}(\theta)] - \Delta[\nabla \cdot F_{ocn}(\theta)],$$
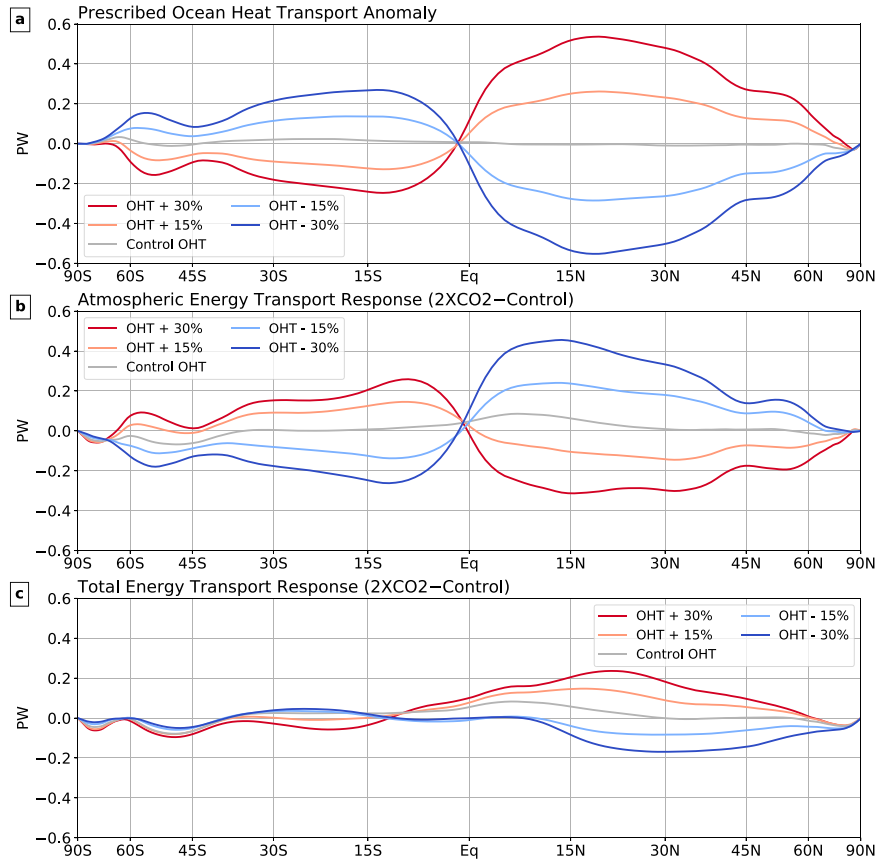
(2)

FIG. 5. Changes in energy transport in the CESM1-SOM CO_2-doubling experiments, relative to the preindustrial: (a) the prescribed ocean heat transport anomaly (PW), (b) the atmospheric energy transport response (PW), and (c) the total energy transport response (PW).

where $R_F(\theta)$ is the (zonal mean) radiative forcing at each latitude θ, $\lambda_i(\theta)$ is the ith local radiative feedback (which includes the Planck, lapse rate, cloud, water vapor, and surface albedo feedbacks), $\Delta T(\theta)$ is the zonal mean surface warming, $-\nabla \cdot F_{\text{atm}}(\theta)$ is the meridional atmospheric energy transport convergence, and $-\nabla \cdot F_{\text{ocn}}(\theta)$ is the meridional ocean heat transport convergence. In general, the product $\lambda_i(\theta)\Delta T(\theta)$ is the top-of-the-atmosphere radiative anomaly due to the ith feedback.

To derive the warming contributions due to each of these terms, we explicitly write out the top-of-the-atmosphere anomaly due to each of the feedbacks λ_i:

$$\sum_i \lambda_i \Delta T = (\lambda_{\text{Pl}} + \lambda_{\text{LR}} + \lambda_{\text{WV}} + \lambda_{\text{Cl}} + \lambda_{\text{Al}})\Delta T, \quad (3)$$

where λ_{Pl} is the Planck feedback, λ_{LR} is the lapse rate feedback, λ_{WV} is the total water vapor feedback (which includes longwave and shortwave components), λ_{Cl} is the total cloud feedback (which also includes longwave and shortwave components), and λ_{Al} is the surface albedo feedback. Note that while λ_i and ΔT are a function of latitude θ, we have dropped this spatial notation for the sake of clarity.

We decompose the Planck feedback, λ_{Pl} into a global mean component $\overline{\lambda_{\text{Pl}}}$ and its spatial deviation λ'_{Pl}:

$$\lambda_{\text{Pl}} = \overline{\lambda_{\text{Pl}}} + \lambda'_{\text{Pl}}. \quad (4)$$

The global mean Planck feedback $\overline{\lambda_{\text{Pl}}}$ is the reference feedback parameter in the climate system, i.e., the top-of-the-atmosphere energy loss per degree of warming in the absence of other feedbacks. We use this decomposition of the Planck feedback, along with Eqs. (3) and (2), to write the total temperature change ΔT as a sum of contributions from feedbacks, the forcing, and changes in energy transports (Feldl and Roe 2013; Goosse et al. 2018):

$$\Delta T = -\frac{(\lambda'_{\text{Pl}} + \lambda_{\text{LR}} + \lambda_{\text{WV}} + \lambda_{\text{Cl}} + \lambda_{\text{Al}})\Delta T}{\overline{\lambda_{\text{Pl}}}}$$
$$-\frac{R_f}{\overline{\lambda_{\text{Pl}}}} - \frac{\Delta(\nabla \cdot F_{\text{atm}})}{\overline{\lambda_{\text{Pl}}}} - \frac{\Delta(\nabla \cdot F_{\text{ocn}})}{\overline{\lambda_{\text{Pl}}}}. \quad (5)$$

The zonal mean temperature changes attributable to each of the radiative feedbacks λ_i are shown in Figs. 8g–l and 9d–f, with globally and regionally averaged temperature changes given in Table 1. Over the globe, differences in water vapor
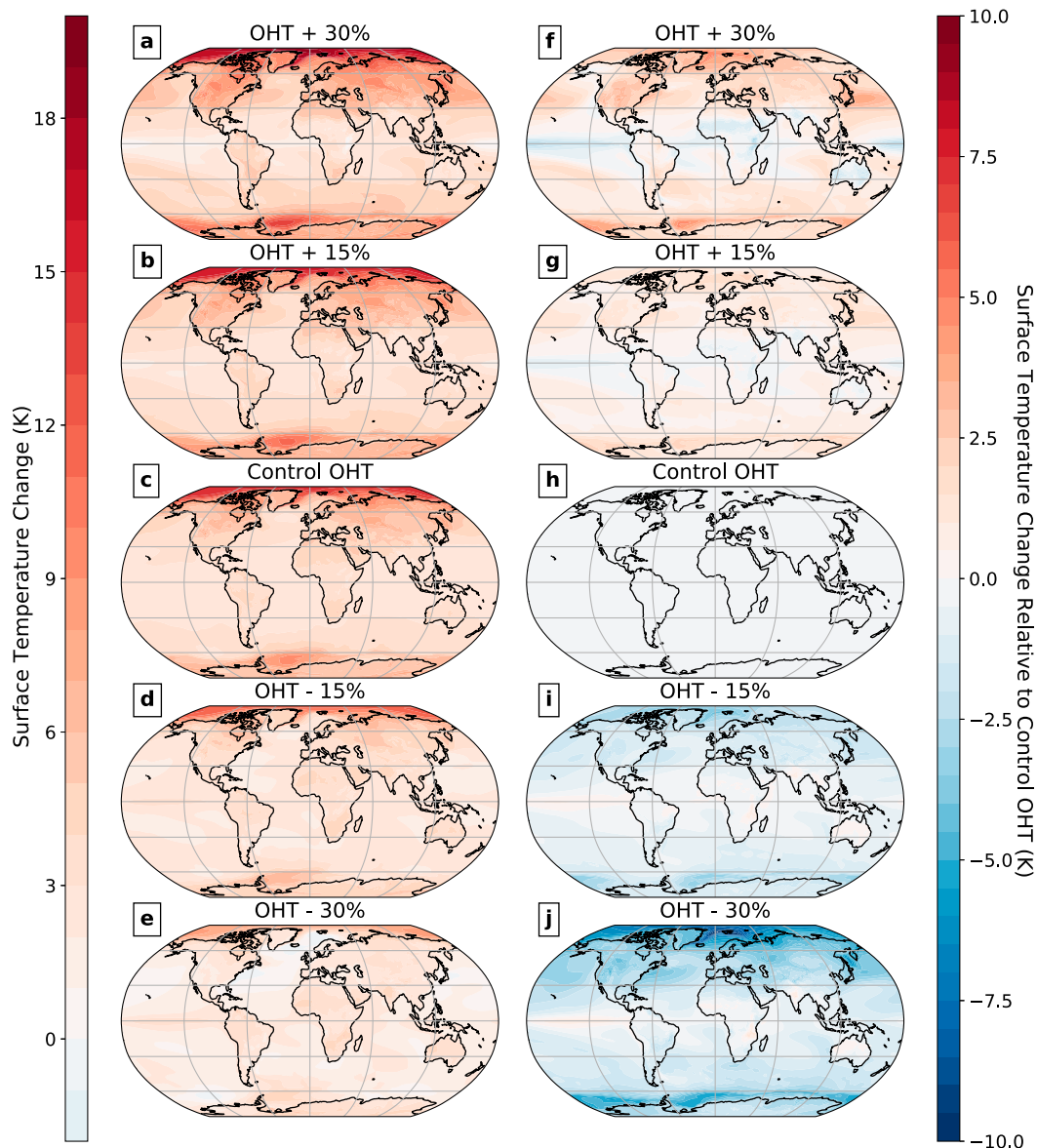
FIG. 6. Change in surface temperature in the CESM1-SOM CO_2-doubling experiments: (a)–(e) relative to the preindustrial control and (f)–(j) relative to Control OHT.

(Fig. 8i) are most responsible for greater warming in the OHT + 30% and OHT + 15% experiments (where prescribed poleward OHT increases with CO_2 doubling), and weaker warming in the OHT − 30% and OHT − 15% experiments (where prescribed poleward OHT decreases with CO_2 doubling). Indeed, differences in the traditional water vapor feedback cause 1.2 K of spread in global warming between experiments (Table 1), which is half of the 2.4 K total spread in climate sensitivity. Moreover, differences in water vapor feedback contribute substantively to the spread in warming at nearly all latitudes. In the tropics (equatorward of 30°S and 30°N), differences in the traditional water vapor feedback contribute approximately 1.2 K to the spread in surface

warming, nearly all the spread between experiments. In the extratropics (poleward of 30°S and 30°N), differences in the traditional water vapor feedback contribute approximately 1.3 K to the spread in the climate sensitivity, which is about a third of the spread between experiments (Table 1).

In addition to differences in water vapor feedback, both differences in atmospheric lapse rate and surface albedo feedbacks also contribute to the spread in warming between experiments (Figs. 8h,k, respectively), albeit primarily in the extratropics (Table 1). Differences in the atmospheric lapse rate and surface albedo feedbacks are each responsible for about 0.5 K of the spread in (global) climate sensitivity between experiments, and 1.0 K of the spread in extratropical
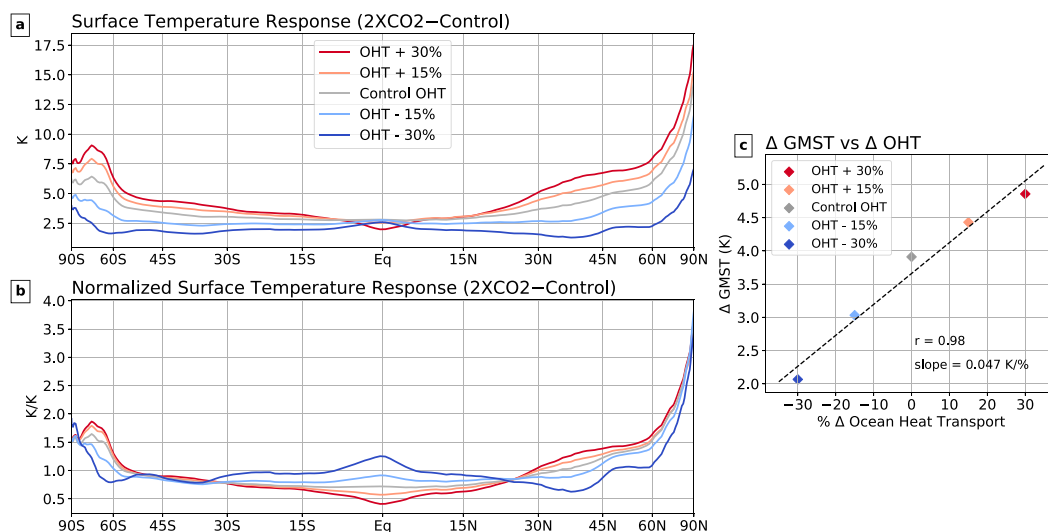
FIG. 7. Change in surface temperature in the CESM1-SOM CO_2-doubling experiments, relative to the preindustrial control: (a) zonal mean change in surface temperature (K), (b) zonal mean change in surface temperature normalized by the global mean change in surface temperature ($K \ K^{-1}$), and (c) percent change in ocean heat transport (relative to the preindustrial control OHT) vs the change in global mean surface temperature, with the line of best fit (dashed).

warming. Differences in surface albedo feedback contribute little to the spread in warming in the tropics, while differences in the traditional lapse rate feedback contribute about 0.1 K to the spread in warming in the tropics.

On thermodynamic grounds, changes in upper-tropospheric specific humidity are not generally separable from changes in temperature (Held and Shell 2012). Therefore, we also quantify contributions to the warming derived from feedbacks using relative humidity as a state variable (Figs. 9d–f and Table 1). This alternative framework provides additional insights on how the spread in warming between CESM1-SOM experiments is governed by changes in water vapor. In the tropics, warming and constant RH moistening do not contribute substantially to the spread in warming between experiments, since the spread due to the Planck curvature and lapse rate feedbacks are small and opposing in sign (Figs. 9d,e; Table 1). Instead, differences in tropical surface warming between experiments are attributable to changes in relative humidity (Fig. 9f; Table 1); specifically, subtropical relative humidity increases when poleward OHT increases with CO_2 doubling (as in the OHT + 15% and OHT + 30% experiments). Indeed, differences in relative humidity account for about one-third of the spread in global mean warming between experiments (Table 1), highlighting the prominent role of relative humidity in modulating climate sensitivity (see, e.g., Bourdin et al. 2021). In the extratropics, on the other hand, changes in water vapor in our experiments mostly occur with vertically nonuniform warming at constant RH, so the spread in warming between experiments is primarily attributable to the constant RH lapse rate feedback, not the RH water vapor feedback (1.2 K spread in extratropical warming is explained by the constant RH lapse rate feedback,

compared to only 0.4 K spread explained by the RH water vapor feedback; see Figs. 9e,f and Table 1).

Most notably, the cloud feedback contributes little to the spread in warming between experiments, both globally and regionally. Though there are substantial differences in clouds between our experiments (which we describe further in section 3), these differences do not contribute substantively to the spread in warming because longwave and shortwave impacts of cloud reduction cancel each other both globally and regionally (see Table 1; as is possible with loss of both high and low clouds; see, e.g., Zelinka et al. 2012).

Figure 10 shows zonal mean warming contributions from the sum of the feedbacks (Fig. 10b), the forcing (Fig. 10c), the atmospheric energy transport (Fig. 10d), and the prescribed OHT (Fig. 10e) in each of the CESM1-SOM experiments. We find that differences in the radiative feedbacks are most responsible for the spread in warming between experiments: differences in these feedbacks are responsible for all of the spread in the global mean warming, 1.3 K of spread in the tropics, and 3.4 K of spread in the extratropics (Table 1). The forcing with CO_2 doubling, on the other hand, is identical between experiments, so it contributes negligibly to the spread in warming between experiments.

Differences in atmospheric and ocean energy transports, which redistribute energy between the tropics and extratropics, cannot contribute to the spread in warming in the global mean, no matter how much these energy transports differ between experiments. However, they do contribute to this spread regionally, albeit in opposite directions: in the OHT − 30% and OHT − 15% experiments, where (prescribed) poleward OHT decreases, the OHT anomaly warms the tropics but cools the extratropics (Fig. 10e, blue-hued
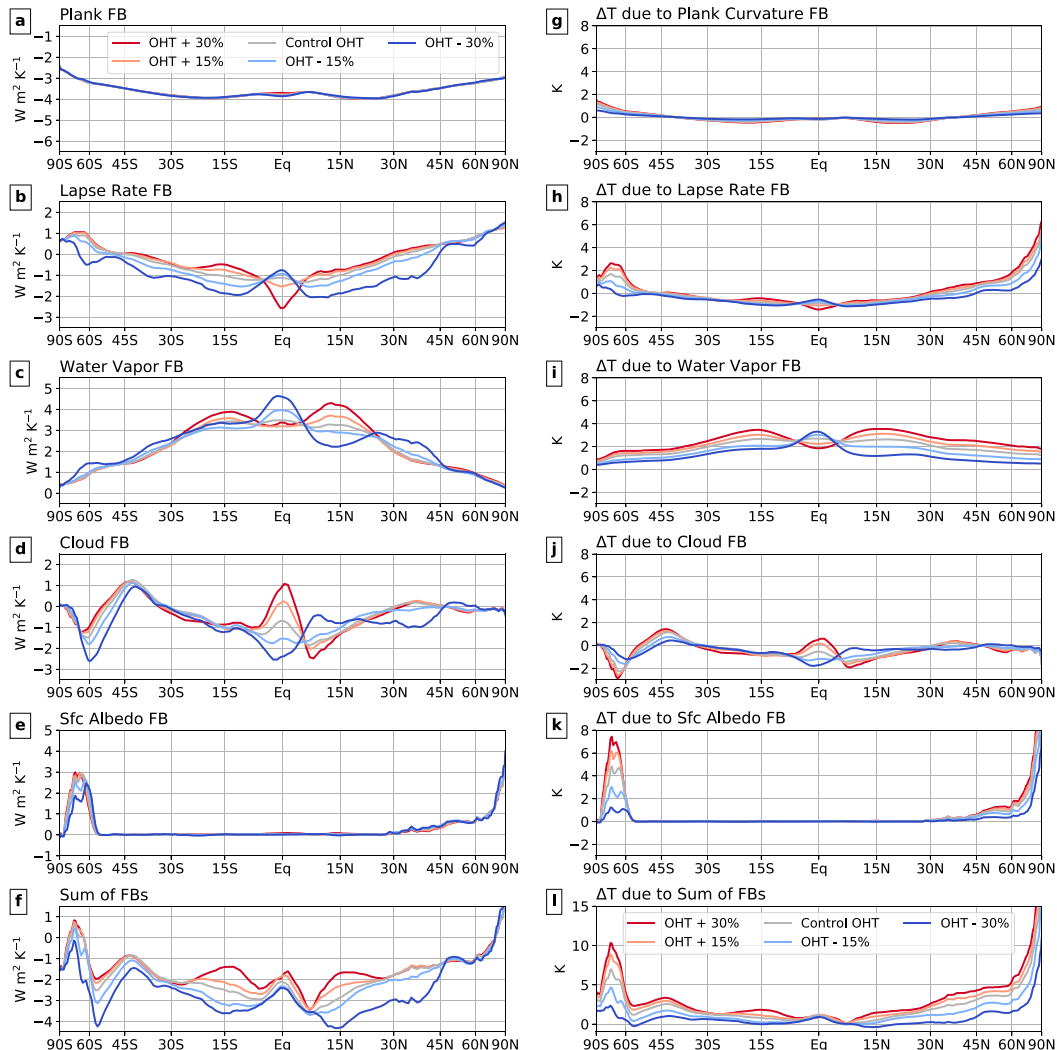
FIG. 8. Zonal mean local radiative feedbacks and temperature changes attributable to these radiative feedbacks in the CESM1-SOM CO_2-doubling experiments: (a)–(e) Plank, lapse rate, total water vapor, total cloud, and surface albedo radiative feedbacks (W m^{-2} K^{-1}); (f) sum of radiative feedbacks (W m^{-2} K^{-1}); and (g)–(k) temperature changes attributable to the Planck curvature, lapse rate feedback, total water vapor feedback, total cloud feedback, and surface albedo feedback (K); and (l) total temperature change attributable to the radiative feedbacks (K).

lines), while the compensating atmospheric energy transport response cools the tropics but warms the extratropics (Fig. 10f, blue-hued lines). Similarly, in the OHT + 30% and OHT + 15% experiments, where poleward OHT increases, the OHT anomaly cools the tropics but warms the extratropics (Fig. 10e, red-hued lines), while the compensating atmospheric energy transport response warms the tropics but cools the extratropics (Fig. 10f, red-hued lines). Overall, the differences in (prescribed) OHT tend to decrease the spread in warming in the tropics, but amplify it in the extratropics, while the differences in the atmospheric energy transport response tend to increase the spread in warming in the tropics but damp it in the extratropics (see Table 1).

Because of how efficiently atmospheric energy transport compensates for changes in OHT (recall Fig. 5), the spread in

warming attributable to differences in the total energy transport change is only about one-third of that due to differences in either OHT or AET alone (cf. Fig. 10g with 10e,f). As described previously (recall Fig. 5), the atmospheric energy transport compensates for about two-thirds of the (prescribed) OHT change; as a result, we find that the regional warming attributable to the total energy transport change is of the same sign as that due to the OHT change, albeit much weaker (Table 1). The total energy transport tends to warm the tropics and cool the extratropics in the OHT − 30% and OHT − 15% experiments (blue-hued lines in Fig. 10g), but tends to cool the tropics and warm the extratropics in the OHT + 30% and OHT + 15% experiments (red-hued lines in Fig. 10g). These differences in the total energy transport between experiments tend to decrease the spread in warming
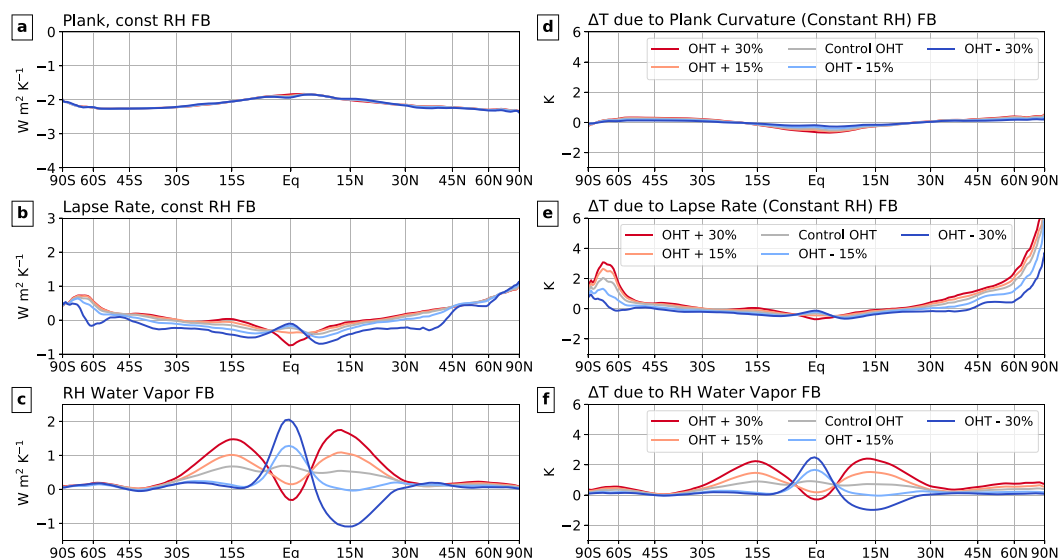
FIG. 9. Zonal mean local radiative feedbacks computed using relative humidity (RH) as the state variable, and temperature changes attributable to these radiative feedbacks in the CESM1-SOM CO_2-doubling experiments: (a)–(c) constant RH Plank, constant RH lapse rate, and RH water vapor radiative feedbacks (W m^{-2} K^{-1}); and (d)–(f) temperature changes attributable to the constant RH Planck curvature, constant RH lapse rate feedback, and RH water vapor feedback (K).

in the tropics by 0.4 K, but increase the spread in warming in the extratropics by 0.4 K.

For completeness, we also show the total temperature change reckoned from Eq. (5) in Fig. 10g (i.e., the sum of warming contributions from radiative feedbacks, forcing, and energy transports), with the residual of this decomposition, relative to the actual warming in the CESM1-SOM experiments (Fig. 10a), shown in Fig. 10h. The decomposition captures the spatial pattern of warming in the different experiments well (cf. Figs. 10a,g), but overestimates the temperature change by about 0.5 K at most latitudes in all experiments. We note that the decomposition accounts for approximately 85% of the spread in warming between experiments, suggesting that it provides a reasonable accounting of warming contributions from feedbacks, forcing, and energy transports.

Thus, our analysis of energetics suggests that differences in radiative feedbacks are responsible for nearly all the spread in warming between CESM1-SOM experiments in the global mean, and most of the spread by region. Indeed, differences in energy transports only contribute modestly to regional differences in warming because of how efficiently atmospheric energy transport compensates for changes in OHT. However, we emphasize that differences in how radiative feedbacks contribute to warming in the CESM1-SOM experiments can only be due to differences in the (prescribed) OHT response to CO_2 doubling, and the corresponding atmospheric energy transport response. Differences in OHT in our experiments give rise to differences in atmospheric and surface properties, which impact the radiative feedbacks and the warming they engender. This suggests that the warming impact of dynamics, namely, atmospheric and ocean energy transports, and the

warming impact of radiative feedbacks cannot necessarily be considered to be independent of each other. A key question that remains is exactly how changes in energy transports impact the atmospheric and surface properties described, namely, atmospheric water vapor, lapse rate, and the surface albedo, and hence the radiative feedbacks. We address this important question in the next section.

3) HOW CHANGING ENERGY TRANSPORTS IMPACT RADIATIVE FEEDBACKS

We now seek to understand how differences in OHT, and compensating differences in atmospheric energy transport, cause differences in water vapor, lapse rate, and surface albedo, and hence differences in radiative feedbacks between our CESM1-SOM experiments. To begin our inquiry, it is useful to consider how the atmospheric circulation responds to CO_2 doubling differently when poleward OHT differs.

Figures 11a–c shows the change in the Eulerian mass overturning streamfunction in the OHT + 30%, Control OHT, and OHT − 30% experiments, respectively. With CO_2 doubling and no accompanying changes in poleward OHT (as in Control OHT), the Hadley cells in both hemispheres weaken and expand (colors in Fig. 11b), a phenomenon that has been described previously as a response to CO_2-forcing (see Lu et al. 2007). When poleward OHT increases with CO_2 doubling, as in the OHT + 30% experiment, the Hadley cells weaken even more substantially than in the Control OHT experiment (cf. Figs. 11a,b). Conversely, when poleward OHT decreases with CO_2 doubling, as in the OHT − 30% experiment, the Hadley circulation does not weaken (Fig. 11c); instead, the rising branch of the Northern Hemispheric Hadley cell strengthens. These atmospheric dynamic

TABLE 1. Attribution of surface temperature change in the CESM1-SOM CO_2-doubling experiments to radiative feedbacks (Planck curvature, lapse rate, water vapor, surface albedo, and cloud), CO_2 forcing, ocean heat transport, and atmospheric energy transport, as delineated by Eq. (5). Shown averaged over the globe, tropics (from 30°S to 30°N), and extratropics (poleward of 30°S and 30°N). "Spread in ΔT" column denotes the difference between the ΔT contributions in OHT + 30% and OHT − 30%; positive values indicate that the factor increases the spread in warming between OHT + 30% and OHT − 30%, while negative values indicate that the factor decreases the spread. Quantities in parentheses indicate warming contributions and spread computed with feedbacks using relative humidity as the state variable (see Held and Shell 2012).

	CESM1-SOM experiment					
	OHT + 30%	OHT + 15%	Control OHT	OHT − 15%	OHT − 30%	Spread in ΔT
Global ΔT						
Total feedback	3.04	2.60	2.14	1.43	0.70	2.34
Planck curvature (constant-RH)	0.00 (0.00)	0.00 (0.00)	0.00 (0.00)	0.00 (0.00)	0.00 (0.00)	0.00 (0.00)
Lapse rate FB (constant-RH)	0.21 (0.66)	0.11 (0.55)	−0.01 (0.41)	−0.19 (0.21)	−0.39 (0.04)	0.60 (0.62)
Water vapor FB (change in RH)	2.48 (0.90)	2.22 (0.64)	1.99 (0.47)	1.62 (0.26)	1.27 (0.14)	1.21 (0.76)
Surface albedo FB	0.75	0.66	0.57	0.41	0.22	0.53
Cloud FB	−0.40	−0.39	−0.41	−0.41	−0.41	0.01
Forcing	1.74	1.74	1.73	1.73	1.74	0.00
Tropical $\Delta\Delta T$ (30°S–30°N)						
Total feedback	1.31	1.06	0.81	0.49	0.18	1.13
Planck curvature (constant-RH)	−0.31 (−0.25)	−0.29 (−0.23)	−0.26 (−0.20)	−0.2 (−0.16)	−0.14 (−0.11)	−0.17 (−0.14)
Lapse rate FB (constant-RH)	−0.67 (−0.16)	−0.69 (−0.19)	−0.75 (−0.24)	−0.80 (−0.29)	−0.85 (−0.34)	0.18 (0.18)
Water vapor FB (change in RH)	2.94 (1.34)	2.71 (0.94)	2.51 (0.69)	2.14 (0.38)	1.78 (0.19)	1.16 (1.15)
Surface albedo FB	0.03	0.02	0.02	0.02	0.01	0.02
Cloud FB	−0.68	−0.69	−0.71	−0.66	−0.63	−0.05
Forcing	1.82	1.82	1.82	1.82	1.82	0.00
Total transport	−0.21	−0.11	0.02	0.12	0.22	−0.43
Ocean heat transport	−0.72	−0.36	0.02	0.40	0.76	−1.48
Atmospheric energy transport	0.49	0.25	0.00	−0.28	−0.54	1.03
Extratropical ΔT (90°–30°S, 30°–90°N)						
Total feedback	4.79	4.16	3.49	2.38	1.22	3.57
Planck curvature (constant-RH)	0.31 (0.25)	0.29 (0.23)	0.26 (0.21)	0.20 (0.16)	0.14 (0.11)	0.17 (0.14)
Lapse rate FB (constant-RH)	1.09 (1.49)	0.92 (1.29)	0.74 (1.07)	0.43 (0.71)	0.06 (0.28)	1.03 (1.21)
Water vapor FB (change in RH)	2.02 (0.47)	1.74 (0.34)	1.47 (0.25)	1.10 (0.15)	0.76 (0.08)	1.26 (0.39)
Surface albedo FB	1.48	1.31	1.12	0.81	0.44	1.04
Cloud FB	−0.11	−0.09	−0.10	−0.16	−0.18	0.07
Forcing	1.65	1.65	1.65	1.65	1.65	0.00
Total transport	0.21	0.08	−0.04	−0.13	−0.23	0.44
Ocean heat transport	0.70	0.33	−0.04	−0.41	−0.78	1.48
Atmospheric energy transport	−0.49	−0.25	0.00	0.28	0.55	−1.04

responses in the OHT + 30% and OHT − 30% experiments correspond to a weakening and strengthening of the tropical atmospheric circulation, respectively, which is consistent with the efficient energy transport compensation described previously (recall Fig. 5).

These differences in how the atmospheric circulation responds to CO_2 doubling in our experiments are particularly evident in the atmospheric vertical velocity ("omega," in Pa h^{-1}; Figs. 11d–f) and cloud cover (Figs. 11g–i). When poleward OHT increases with CO_2 doubling, as in the OHT + 30% experiment, deep convection near the equator weakens and subsidence in the subtropics declines (Fig. 11d), reflecting the profound weakening of the Hadley circulation in this experiment; as a result, clouds decline near the equator, but increase in the subtropics (Fig. 11g). Similarly, we also find that deep convection near the equator weakens and subsidence in the subtropics declines in the Control OHT experiment (Fig. 11e), albeit more modestly than in the OHT + 30% experiment. On the other hand, when poleward OHT

declines with CO_2 doubling as in the OHT − 30% experiment, equatorial deep convection strengthens (Fig. 11f), and clouds increase in the deep tropics (Fig. 11i).

We now show how differences in the atmospheric circulation response, along with (prescribed) differences in OHT, increase atmospheric water vapor in the OHT + 30% and OHT + 15% experiments, leading to greater warming, and decrease atmospheric water vapor in the OHT − 30% and OHT − 15% experiments, leading to weaker warming. Figures 12a,b, and c show the surface latent heat flux (i.e., evaporation), atmospheric latent heat transport, and column-integrated precipitable water, respectively, in each of the CESM1-SOM experiments. Because atmospheric CO_2 is doubled in all experiments, latent heat fluxes increase at most latitudes, and column-integrated precipitable water increases globally. However, differences in evaporation and the strength of the atmospheric circulation give rise to very different amounts of column-integrated precipitable water in each of the experiments.
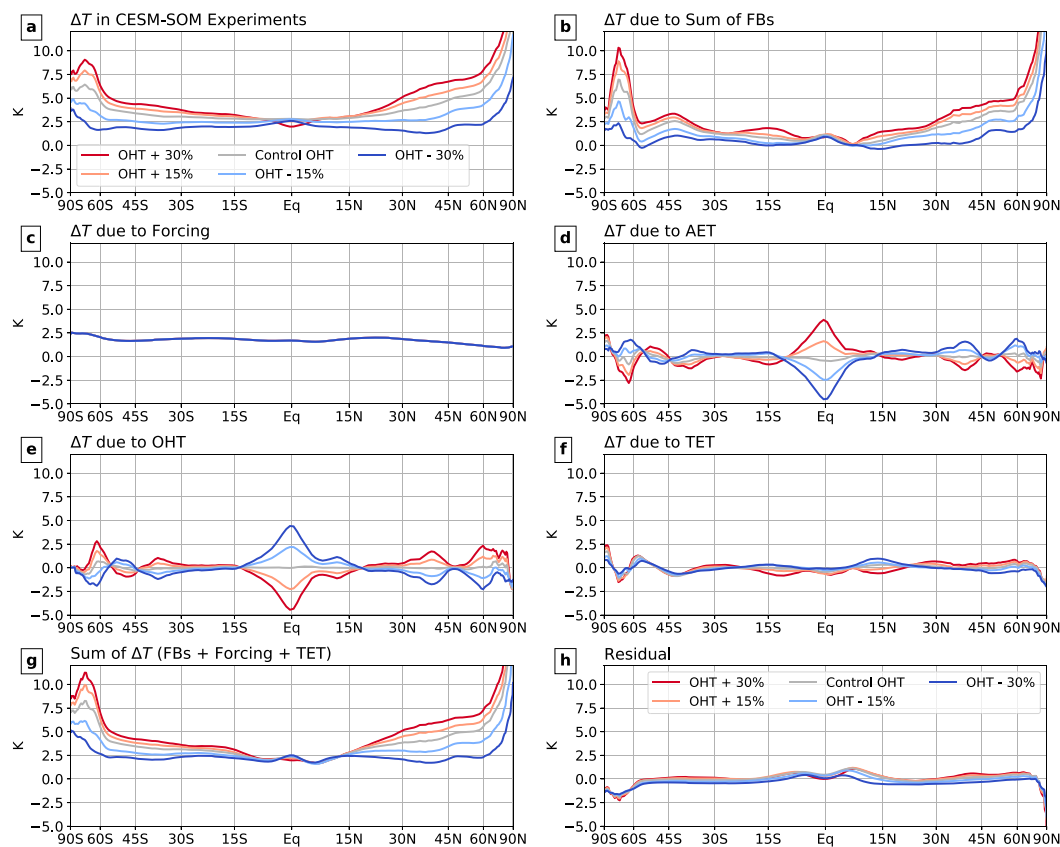
FIG. 10. Feedback, forcing, and energy transport contributions to the zonal mean temperature change (K) in the CESM1-SOM CO_2-doubling experiments: (a) zonal mean temperature change; (b) temperature change attributable to the sum of radiative feedbacks; (c) temperature change attributable to the forcing (in the absence of radiative feedbacks); (d) temperature change due to changes in the atmospheric energy transport; (e) temperature change due to (prescribed) changes in ocean heat transport; (f) temperature change due to changes in the total energy transport; (g) sum of temperature change contributions from the feedbacks, forcing, and total energy transport; and (h) the residual of the decomposition [i.e., the difference between (a) and (g)].

In the experiments with weaker poleward OHT, OHT − 30%, and OHT − 15%, weaker evaporation and a more vigorous atmospheric circulation both moderate how much atmospheric precipitable water increases with CO_2 doubling. In these experiments, there is more convergence of ocean heat equatorward of 15°N and 15°S, and less convergence of ocean heat poleward of 15°N and 15°S. Prior studies have shown that greater ocean heat convergence in the mixed layer impacts the atmosphere through greater turbulent heat loss, notably greater latent heat fluxes (Hartmann 1994; Sutton and Mathieu 2002). This relationship between ocean heat convergence and latent heat fluxes is evident in Fig. 12a, which shows that experiments with weaker poleward OHT have stronger evaporation equatorward of 15°N/ 15°S, and weaker evaporation poleward of 15°N/15°S (blue-hued lines). Weaker evaporation poleward of 15°N/15°S leads to less precipitable water in the extratropics in these experiments (blue-hued lines in Fig. 12c). In the deep tropics, however, greater evaporation and a more vigorous atmospheric circulation both augment latent heat transport

toward the intertropical convergence zone (ITCZ; blue-hued lines in Fig. 12b), which leads to a peak in atmospheric precipitable water near the equator (Fig. 12c, blue-hued lines) and a pronounced peak in precipitation sensitivity (Fig. 12d, blue-hued lines). Overall, weaker latent heat fluxes in the extratropics, combined with more vigorous moisture transport away from the subtropics toward regions of deep convection at the ITCZ, leads to less water vapor in the OHT − 30% and OHT − 15% experiments and, therefore, less warming.

In the OHT + 30% and OHT + 15% experiments, where (prescribed) poleward OHT strengthens with CO_2 doubling, we find a nearly opposing set of processes that act in concert to increase atmospheric precipitable water. Greater ocean heat convergence poleward of 15°N/15°S increases evaporation in the extratropics (Fig. 12a, red-hued lines) and, therefore, also increases precipitable water in the extratropics (Fig. 12c, red-hued lines). In the tropics, a sluggish atmospheric overturning circulation only weakly converges precipitable water toward the ITCZ, causing atmospheric
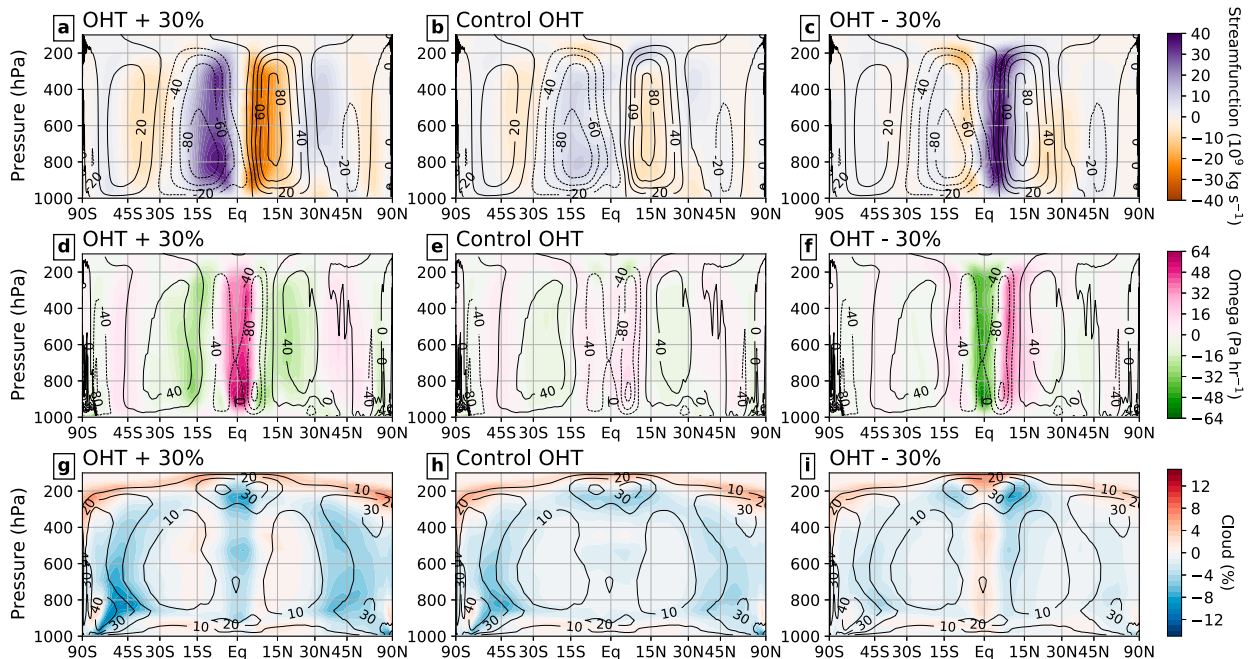
FIG. 11. Atmospheric circulation and cloud responses in the OHT + 30%, Control OHT, and OHT − 30% CESM1-SOM CO_2-doubling experiments, relative to the preindustrial control: (a)–(c) change in the Eulerian mass overturning streamfunction (10^9 kg s^{-1}; colors), shown with the preindustrial control mass overturning streamfunction (contours); (d)–(f) change in the zonal mean atmospheric vertical velocity "omega" (Pa h^{-1}; colors), shown with the atmospheric vertical velocity in the preindustrial control (contours); and (g)–(i) change in clouds (%; colors), shown with cloud cover in the preindustrial control (contours).

precipitable water to accumulate in the subtropics (see maxima in precipitable water circa 10°N and 10°S in Fig. 12c, red-hued lines). Indeed, the atmospheric circulation is so weak in the OHT + 30% and OHT + 15% experiments that precipitation at the ITCZ actually declines (red-hued lines in Fig. 12d). Therefore, both greater evaporation in the extratropics and a weaker atmospheric circulation in the tropics contribute to greater atmospheric precipitable water, more water vapor, and greater warming when poleward OHT increases with CO_2 doubling.

Differences in atmospheric circulation strength also cause differences in the lapse rate in the tropics and midlatitudes in our CESM1-SOM experiments, which also leads to differences in surface warming. This is demonstrated in Fig. 13, where we show how specific humidity, moist potential temperature, and atmospheric temperature (normalized relative to global mean warming) respond to CO_2 doubling in the OHT + 30%, Control OHT, and OHT − 30% experiments.

When poleward OHT increases, as in the OHT + 30% experiment, the Hadley cells weaken substantially with CO_2 doubling (recall Fig. 11a). As a result, low-level moisture convergence to the ITCZ decreases, deep convection weakens, and specific humidity increases very little near the equator (Fig. 13a). Because deep convection is weak near the equator, air with high moist static energy (i.e., of high moist potential temperature) does not rise to the upper troposphere; indeed, moist potential temperature increases most near the subtropical and midlatitude surface in this experiment, not the upper troposphere (Fig. 13d). Consequently, the tropical and

midlatitude upper troposphere only warms modestly relative to warming at the surface (Fig. 13g). Weaker warming aloft, relative to the surface, leads to a less negative lapse rate feedback, which produces more surface warming when poleward OHT increases with CO_2 doubling (as in the OHT + 30% and OHT + 15% experiments).

On the other hand, when poleward OHT decreases (as in the OHT − 30% experiment), we find that an opposing set of processes tends to increase warming aloft in the tropics and midlatitudes, which helps decrease surface warming (recall warming contributions from the lapse rate feedback in OHT − 15% and OHT − 30%, Table 1). When poleward OHT decreases, the tropical circulation remains vigorous (recall Fig. 11c), low-level moisture convergence at the ITCZ increases (recall Fig. 12b), and deep convection carries more moisture aloft in the deep tropics (Fig. 13c). Deep convection near the equator moves air with high moist static energy from the surface to the upper troposphere (Fig. 13f), which effectively warms the upper troposphere relative to the surface (Fig. 13i). Such greater warming aloft, relative to the surface, leads to a more negative lapse rate feedback, which decreases surface warming in the OHT − 15% and OHT − 30% experiments.

Finally, at subpolar and polar latitudes, we find that differences in lapse rate and surface albedo between CESM1-SOM experiments are caused by differences in how snow and ice respond to CO_2 doubling. Figure 14 shows the change in snow (on land) and sea ice (on ocean) in each experiment over the Arctic (Figs. 14a–e) and Antarctic (Figs. 14f–j). In all experiments, sea ice area and snow depths decline, as expected with
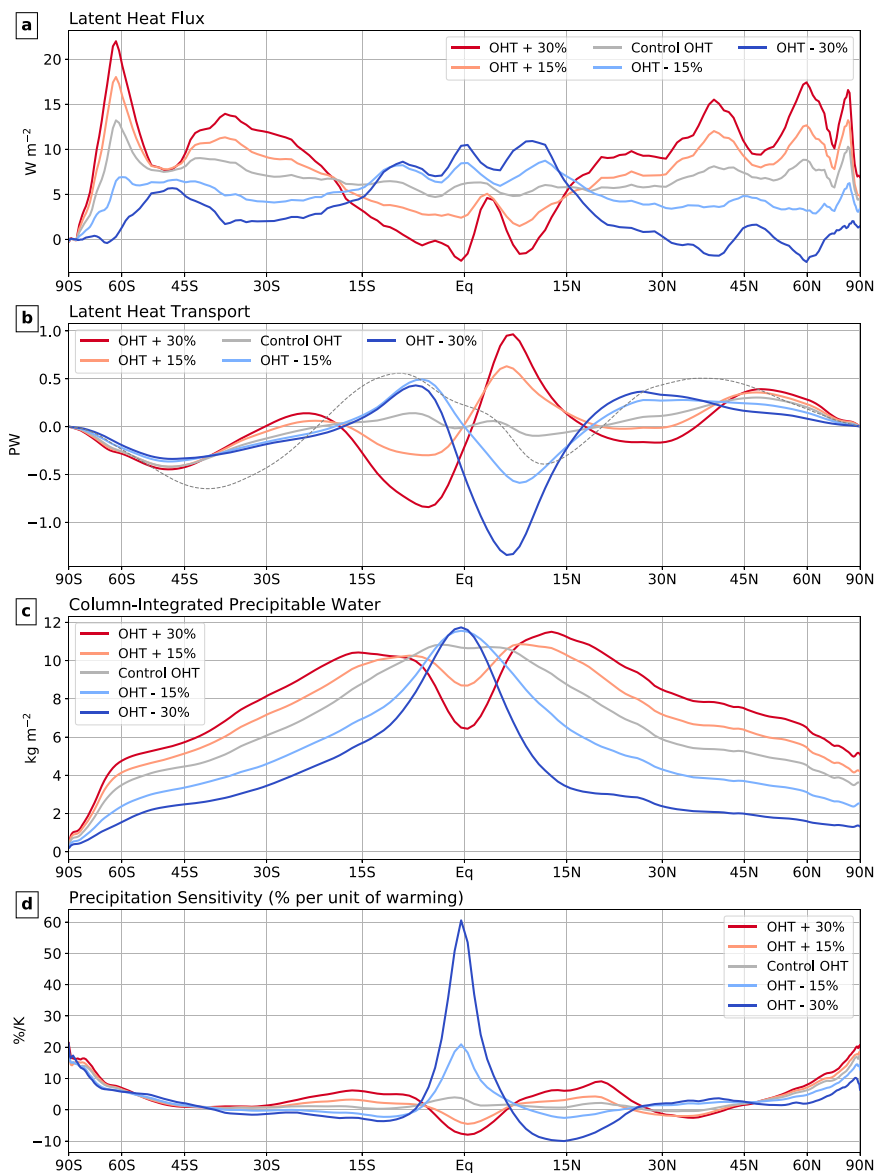
FIG. 12. Zonal mean change in the atmospheric hydrologic cycle in the CESM1-SOM CO_2-doubling experiments, relative to the preindustrial control: (a) change in the surface latent heat flux (W m^{-2}); (b) change in the latent heat transport (in PW; the black dotted line shows the latent heat transport in the preindustrial control, scaled by a factor of 0.1); (c) change in column-integrated precipitable water (kg m^{-2}); and (d) the precipitation sensitivity, the percentage change in precipitation relative to the global mean surface temperature change (% K^{-1}).

CO_2 forcing. However, in experiments with increased poleward OHT (OHT + 30% and OHT + 15%), sea ice area and snow depths decline more (Figs. 14a,b and f,g), and in experiments with decreased poleward OHT (OHT − 30% and OHT − 15%), sea ice area and snow depths decline less (Figs. 14d,e and i,j).

Prior studies have shown that greater ocean heat convergence into the polar regions is correlated with decreased sea ice cover and amplified high-latitude warming (Holland and Bitz 2003; Hwang et al. 2011). Our experiments show that this relationship

can be causative (as found in Singh et al. 2017): greater poleward OHT (corresponding to greater ocean heat convergence into the high-latitude oceans) causes greater sea ice loss (compare, for example, Figs. 14a,e), a more positive surface albedo feedback, and, therefore, more polar-amplified warming (recall warming attributable to the surface albedo feedback in Table 1). More polar-amplified warming further increases rainfall, at the expense of snowfall, and decreases the persistence of snow cover, particularly over the mid- and high latitudes in the Northern Hemisphere (see Brown and Mote 2009).
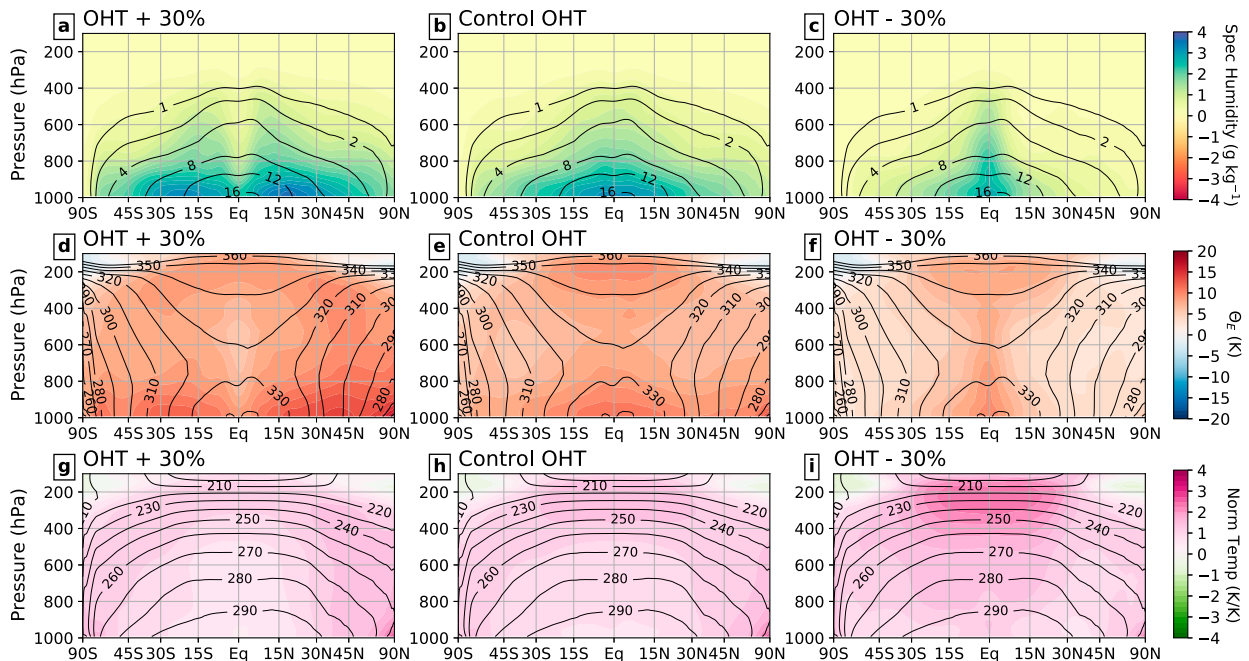
FIG. 13. Atmospheric specific humidity, moist entropy, and normalized temperature responses in the OHT + 30%, Control OHT, and OHT − 30% CESM1-SOM CO_2-doubling experiments, relative to the preindustrial control: (a)–(c) change in the atmospheric specific humidity (g kg^{-1}; colors), shown with the preindustrial control specific humidity (contours); (d)–(f) change in the moist potential temperature (K; colors), shown with the moist potential temperature in the preindustrial control (contours); and (g)–(i) change in the atmospheric temperature, normalized by the global mean surface warming (K K^{-1}; colors), shown with the atmospheric temperature in the preindustrial control (K; contours).

Additionally, studies show that sea ice loss also amplifies the (positive) lapse rate feedback in the high latitudes by warming the lower troposphere in winter (Manabe and Stouffer 1980; Deser et al. 2015; Feldl et al. 2020). This is also evident in our CESM1-SOM experiments, where we find that experiments with greater ice loss (like OHT + 30%) experience more surface-amplified warming in the high latitudes (Fig. 13g) and, consequently, more warming attributable to the lapse rate feedback (recall Fig. 8 and Table 1). Thus,

differences in sea ice loss between experiments are driven by differences in poleward OHT, which impact warming through effects on both lapse rate and surface albedo.

4. Discussion

Our results provide compelling evidence that changes in ocean heat transport, concomitant with CO_2-forcing, impact equilibrium climate sensitivity. Notably, we find that even
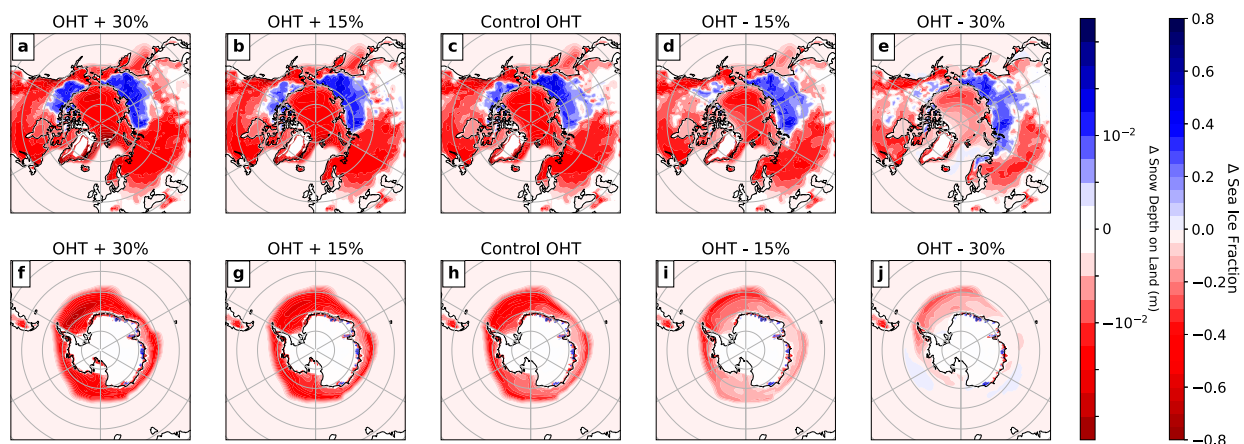

FIG. 14. Change in snow cover depth (over land; in m) and sea ice fraction in the CESM1-SOM CO_2-doubling experiments: (a)–(e) changes in the Arctic and (f)–(j) changes in the Antarctic.

though OHT changes are opposed by the atmosphere, both ocean and atmosphere energy transport changes together impact climate sensitivity through their impact on radiative feedbacks, specifically the water vapor, surface albedo, and lapse rate feedbacks. When poleward OHT increases with CO_2 doubling, atmospheric water vapor increases more outside of the deep tropics, warming is more surface amplified, and sea ice (and snow cover) decrease more. Conversely, when poleward OHT declines with CO_2 doubling, atmospheric water vapor increases much less outside of the deep tropics, warming is more pronounced in the upper troposphere, and sea ice (and snow cover) only decline modestly. These factors, namely, water vapor, lapse rate, and sea ice, act in concert to amplify climate sensitivity when poleward OHT increases, and to damp climate sensitivity when poleward OHT declines.

These results have important implications for climate change research. As we have shown, most Earth system models simulate a decline in poleward OHT when forced with CO_2 (recall Fig. 1). In the Northern Hemisphere, this decline in poleward OHT is weakly correlated with the extent of warming in that hemisphere (recall Fig. 2), but such a correlation does not preclude the possibility that the magnitude of OHT change simply scales with warming and does not help drive it. However, our experiments using CESM1-SOM show that a concomitant decline of poleward OHT with CO_2 doubling, as in OHT − 15% (which most closely follows the decline in poleward OHT in the fully coupled CESM1), can decrease the equilibrium climate sensitivity by nearly 1 K (recall Fig. 7). Moreover, the relationship between poleward OHT changes (at 45°N) and warming is similar in magnitude in the models we examined in the CMIP6 multimodel ensemble, the fully coupled CESM1, and the CESM1 slab ocean model experiments: all exhibit a slope between 0.05 and 0.1 PW K^{-1}, suggesting that similar mechanisms likely operate over a variety of forcings and a range of time scales. Therefore, our results show that changes in poleward OHT are not merely an indicator of greater or weaker warming, but are also a factor that can determine the magnitude of warming. Further analysis of fully coupled, transient, CO_2-forced Earth system model experiments (such as SSP585 in CMIP6) could more fully elucidate the extent that decreased poleward OHT may moderate transient warming due to CO_2 forcing, and may therefore act as a negative feedback on the climate system response over a range of time scales.

Results of our CESM1-SOM experiments are not only applicable to present-day climate change, but also to climates of the distant past. Our experiments suggest that a warmer climate, and a weaker pole-to-equator temperature gradient, are possible if poleward OHT increases as atmospheric greenhouse gases increase. This finding is in alignment with the study of Rose and Ferreira (2013), who showed that the "low-gradient paradox," the observation that the pole-to-equator temperature gradient was likely much weaker in past hothouse climates (like that of the Cretaceous or early Paleogene) than is possible to achieve in most climate models (see, e.g., Caballero and Langen 2005), could be largely reconciled if poleward OHT were to increase (relative to the

present-day) in such climate states. Indeed, we find that increased poleward OHT is effective at increasing climate sensitivity and decreasing the pole-to-equator temperature gradient by augmenting atmospheric water vapor in the extratropics, weakening the atmospheric circulation, and melting sea ice cover. However, we also note that increased poleward OHT appears to be less effective at amplifying climate sensitivity than decreasing poleward OHT is at moderating it (recall Fig. 7). Similarly, Barreiro et al. (2011) found that increasing poleward OHT substantially beyond that of the present-day may actually cool the planet through increased low cloud cover in the tropics. Whether this asymmetry in the climate system response to changes in OHT is merely a function of the base state climate, or implies that far higher greenhouse gas concentrations are required to sustain such low-gradient climates, requires further study.

An important finding of our study is that changes in energy transports, both atmospheric and ocean, impact climate sensitivity through their effect on radiative feedbacks. We find that radiative feedbacks cause less global warming when poleward OHT decreases with CO_2 doubling, and more global warming when poleward OHT increases with CO_2 doubling. Thus, even though changes in atmospheric and ocean energy transports by themselves cannot impact warming globally (as they only redistribute energy meridionally), they do impact how much the globe warms through their effect on the radiative feedbacks, particularly the water vapor, lapse rate, and surface albedo feedbacks. This finding suggests that column model approaches for estimating radiative feedbacks (see e.g., Koll and Cronin 2018; Seeley and Jeevanjee 2021) are inherently limited as they cannot capture the complex interactions between the general circulation, both atmospheric and ocean, and the radiative feedbacks. This finding also suggests an alternative interpretation for the hypothesis that the spatial pattern of warming determines the radiative feedbacks, irrespective of what processes elicit that pattern of warming (i.e., the pattern effect; see, e.g., Haugstad et al. 2017). In our experiments, differences in ocean heat transport lead to differences in surface heat fluxes that have nonlocal impacts on feedbacks through the atmospheric circulation. These atmospheric circulation changes incited by changes in ocean heat flux convergence can also affect SSTs downstream (Sutton and Mathieu 2002), thereby creating a unique warming pattern. Hence, both the warming pattern and the radiative feedbacks may be a product of (atmospheric and ocean) energy transport anomalies; in other words, the warming pattern may not drive variations in the radiative feedbacks, but may be a response to energy transport changes that also alter the radiative feedbacks.

Moreover, given the primacy of radiative feedbacks in determining both global and regional climate sensitivity, an interesting question then arises: can the strength of radiative feedbacks be disentangled from changing atmospheric and ocean energy transports? Other studies have also suggested that energy transports and feedbacks are interrelated, with many hypothesizing that the strength of radiative feedbacks impacts atmospheric moist static energy transport (see, e.g., Hwang et al. 2011; Zelinka and Hartmann 2012; Feldl et al.

2017). Our results suggest that the opposite relationship may also hold: changes in energy transport, either in the atmosphere or ocean, may alter the strength of radiative feedbacks. Most importantly, the sum of these findings suggests that any analysis of radiative feedbacks, and the warming they engender, will bear some imprint of the accompanying changes in dynamics through the coupling between them.

We note that we are not the first to suggest that changes in ocean heat transport impact the climate system through effects on the atmospheric circulation and water vapor. For example, Herweijer et al. (2005) showed that increased poleward OHT warms surface temperatures through both thermodynamics and dynamics: increased surface evaporation (in the subtropics and extratropics) and redistribution of this evaporated moisture away from the deep tropics by way of a weakened Hadley circulation. Rencurrel and Rose (2018) also highlight a similar mechanism, but attest that increased poleward OHT warms surface temperatures mostly by decreasing low cloud cover in the extratropics. While we also find that increasing poleward OHT exacerbates low cloud loss that occurs with CO_2 doubling (recall Fig. 11), we do not find the resulting cloud feedback to be an important contributor to the spread in warming between our experiments (recall Table 1). This may be due to discrepancies in the vertical distribution of cloud changes: unlike Rencurrel and Rose (2018), who found concurrent low cloud loss and high cloud gain with increased poleward OHT, we find that clouds decline throughout the troposphere, which may explain why we see cancellation of longwave and shortwave cloud feedbacks at most latitudes. Whether this difference between our results and that of Rencurrel and Rose (2018) is due to intermodel differences in cloud physics, or due to differences in climate state brought on by CO_2 doubling in our experiments, requires further investigation.

Finally, we discuss limitations of this research. Most importantly, we recognize that in fully coupled Earth system models, changes in poleward OHT do not necessarily follow the idealized OHT changes we have imposed in our CESM1-SOM experiments. For one, many Earth system models exhibit weakening of the northward cross-equatorial OHT (as the Atlantic meridional overturning circulation weakens; see He et al. 2019); others exhibit an increase in poleward OHT into the northern high latitudes, even as poleward OHT decreases at most other latitudes (Nummelin et al. 2017). This suggests that the fully coupled climate system response may include effects of decreasing poleward OHT (at the lower and midlatitudes), increasing poleward OHT (at the high latitudes), and declining northward cross-equatorial OHT. Nevertheless, in spite of these regional inhomogeneities, CESM1-SOM experiments from previous studies performed with spatially varying patterns of OHT produce warming patterns that are consistent with the results described in this study. Increased OHT to the high latitudes, commonly found in Earth system model experiments subject to CO_2 forcing (see Holland and Bitz 2003; Hwang et al. 2011), amplifies polar warming and sea ice loss in both hemispheres (Singh et al. 2017). Similarly, decreased poleward OHT in the tropics and midlatitudes cools these regions (Singh et al. 2017, 2018);

indeed, a CESM1-SOM experiment performed with OHT derived from a fully coupled CESM1 CO_2-doubling experiment with little net ocean heat uptake (about 0.1 W m^{-2}; OHT computed from years 470 to 500 following CO_2 doubling) exhibited about 0.6 K less warming in the Northern Hemisphere extrapolar regions, equatorward of 70°N, and 0.3 K less warming globally see PertAtm+PertOcn485 in Singh et al. 2018). Further investigation is warranted into how such heterogeneous regional OHT changes impact the atmospheric circulation, radiative feedbacks, and the climate system response to CO_2 forcing.

Some further limitations of this research should also be acknowledged. First, we have only used a single model to investigate how dynamic processes impact climate sensitivity. It is possible that the mechanisms we suggest for how changing atmospheric and ocean energy transports impact surface warming (i.e., through water vapor, lapse rate, and sea ice changes) are model dependent. Similar studies with different models will be useful for establishing whether the modus operandi we present here is robust. Additionally, we point out that we have focused on the equilibrium climate system response to changes in OHT, not the transient response. Understanding the latter will require further investigation to disentangle the effects of changes in ocean heat transport from the effects of transient ocean heat uptake. Nevertheless, despite these important caveats, the results we have presented here suggest that how much the climate warms in response to CO_2 forcing is likely sensitive to changing energy transports, which adds an interesting set of dynamic processes to consider for understanding Earth's climate sensitivity.

REFERENCES

Banks, H. T., and J. M. Gregory, 2006: Mechanisms of ocean heat uptake in a coupled climate model and the implications for tracer based predictions of ocean heat uptake. *Geophys. Res. Lett.*, **33**, L07608, https://doi.org/10.1029/2005GL025352.

Barnett, J., L. S. Evans, C. Gross, A. S. Kiem, R. T. Kingsford, J. P. Palutikof, C. M. Pickering, and S. G. Smithers, 2015: From barriers to limits to climate change adaptation: Path

dependency and the speed of change. *Ecol. Soc.*, **20**, 5, https://doi.org/10.5751/ES-07698-200305.

Barreiro, M., A. Cherchi, and S. Masina, 2011: Climate sensitivity to changes in ocean heat transport. *J. Climate*, **24**, 5015–5030, https://doi.org/10.1175/JCLI-D-10-05029.1.

Bitz, C., P. Gent, R. Woodgate, M. Holland, and R. Lindsay, 2006: The influence of sea ice on ocean heat uptake in response to increasing CO_2. *J. Climate*, **19**, 2437–2450, https://doi.org/10.1175/JCLI3756.1.

——, K. Shell, P. Gent, D. Bailey, G. Danabasoglu, K. Armour, M. Holland, and J. Kiehl, 2012: Climate sensitivity in the Community Climate System Model, version 4. *J. Climate*, **25**, 3053–3070, https://doi.org/10.1175/JCLI-D-11-00290.1.

Bjerknes, J., 1964: Atlantic air-sea interaction. *Advances in Geophysics*, Vol. 10, Academic Press, 1–82, https://doi.org/10.1016/S0065-2687(08)60005-9.

Boé, J., A. Hall, and X. Qu, 2009: Deep ocean heat uptake as a major source of spread in transient climate change simulations. *Geophys. Res. Lett.*, **36**, L22701, https://doi.org/10.1029/2009GL040845.

Bourdin, S., L. Kluft, and B. Stevens, 2021: Dependence of climate sensitivity on the given distribution of relative humidity. *Geophys. Res. Lett.*, **48**, e2021GL092462, https://doi.org/10.1029/2021GL092462.

Brown, R. D., and P. W. Mote, 2009: The response of Northern Hemisphere snow cover to a changing climate. *J. Climate*, **22**, 2124–2145, https://doi.org/10.1175/2008JCLI2665.1.

Caballero, R., and P. L. Langen, 2005: The dynamic range of poleward energy transport in an atmospheric general circulation model. *Geophys. Res. Lett.*, **32**, L02705, https://doi.org/10.1029/2004GL021581.

Charney, J. G., and Coauthors, 1979: *Carbon Dioxide and Climate: A Scientific Assessment*. National Academy of Sciences, 24 pp.

Danabasoglu, G., and P. R. Gent, 2009: Equilibrium climate sensitivity: Is it accurate to use a slab ocean model? *J. Climate*, **22**, 2494–2499, https://doi.org/10.1175/2008JCLI2596.1.

——, S. Bates, B. Briegleb, S. Jayne, M. Jochum, W. Large, S. Peacock, and S. Yeager, 2012: The CCSM4 ocean component. *J. Climate*, **25**, 1361–1389, https://doi.org/10.1175/JCLI-D-11-00091.1.

Deser, C., R. Tomas, and L. Sun, 2015: The role of ocean–atmosphere coupling in the zonal-mean atmospheric response to Arctic sea ice loss. *J. Climate*, **28**, 2168–2186, https://doi.org/10.1175/JCLI-D-14-00325.1.

Eyring, V., S. Bony, G. A. Meehl, C. A. Senior, B. Stevens, R. J. Stouffer, and K. E. Taylor, 2016: Overview of the Coupled Model Intercomparison Project Phase 6 (CMIP6) experimental design and organization. *Geosci. Model Dev.*, **9**, 1937–1958, https://doi.org/10.5194/gmd-9-1937-2016.

Farneti, R., and G. K. Vallis, 2013: Meridional energy transport in the coupled atmosphere–ocean system: Compensation and partitioning. *J. Climate*, **26**, 7151–7166, https://doi.org/10.1175/JCLI-D-12-00133.1.

Feldl, N., and G. Roe, 2013: The nonlinear and nonlocal nature of climate feedbacks. *J. Climate*, **26**, 8289–8304, https://doi.org/10.1175/JCLI-D-12-00631.1.

——, S. Bordoni, and T. M. Merlis, 2017: Coupled high-latitude climate feedbacks and their impact on atmospheric heat transport. *J. Climate*, **30**, 189–201, https://doi.org/10.1175/JCLI-D-16-0324.1.

——, S. Po-Chedley, H. K. Singh, S. Hay, and P. J. Kushner, 2020: Sea ice and atmospheric circulation shape the high-latitude lapse rate feedback. *npj Climate Atmos. Sci.*, **3**, 41, https://doi.org/10.1038/s41612-020-00146-7.

Garuba, O., J. Lu, F. Liu, and H. Singh, 2017: The active role of the ocean in the temporal evolution of climate sensitivity. *Geophys. Res. Lett.*, **45**, 306–315, https://doi.org/10.1002/2017GL075633.

Goosse, H., and Coauthors, 2018: Quantifying climate feedbacks in polar regions. *Nat. Commun.*, **9**, 1919, https://doi.org/10.1038/s41467-018-04173-0.

Grise, K. M., and L. M. Polvani, 2014: Southern Hemisphere cloud-dynamics biases in CMIP5 models and their implications for climate projections. *J. Climate*, **27**, 6074–6092, https://doi.org/10.1175/JCLI-D-14-00113.1.

Hansen, J., A. Lacis, D. Rind, G. Russell, P. Stone, I. Fung, R. Ruedy, and J. Lerner, 1984: Climate sensitivity: Analysis of feedback mechanisms. *Climate Processes and Climate Sensitivity*, *Geophys. Monogr.*, Vol. 29, Amer. Geophys. Union, https://doi.org/10.1029/GM029p0130.

Hartmann, D. L., 1994: *Global Physical Climatology*. Academic Press, 500 pp.

Haugstad, A., K. Armour, D. Battisti, and B. Rose, 2017: Relative roles of surface temperature and climate forcing patterns in the inconstancy of radiative feedbacks. *Geophys. Res. Lett.*, **44**, 7455–7463, https://doi.org/10.1002/2017GL074372.

He, C., Z. Liu, and A. Hu, 2019: The transient response of atmospheric and oceanic heat transports to anthropogenic warming. *Nat. Climate Change*, **9**, 222–226, https://doi.org/10.1038/s41558-018-0387-3.

Held, I. M., and K. M. Shell, 2012: Using relative humidity as a state variable in climate feedback analysis. *J. Climate*, **25**, 2578–2582, https://doi.org/10.1175/JCLI-D-11-00721.1.

Herweijer, C., R. Seager, M. Winton, and A. Clement, 2005: Why ocean heat transport warms the global mean climate. *Tellus*, **57A**, 662–675, https://doi.org/10.3402/tellusa.v57i4.14708.

Holland, M., and C. Bitz, 2003: Polar amplification of climate change in coupled models. *Climate Dyn.*, **21**, 221–232, https://doi.org/10.1007/s00382-003-0332-6.

Hunke, E., and W. Lipscomb, 2010: CICE: The Los Alamos sea ice model, documentation and software user's manual, version 4.1. Tech. Rep. LA-CC-06-012, Los Alamos National Laboratory, 76 pp., https://csdms.colorado.edu/w/images/CICE_documentation_and_software_user's_manual.pdf.

Hurrell, J., and Coauthors, 2013: The Community Earth System Model: A framework for collaborative research. *Bull. Amer. Meteor. Soc.*, **94**, 1339–1360, https://doi.org/10.1175/BAMS-D-12-00121.1.

Hwang, Y.-T., D. Frierson, and J. Kay, 2011: Coupling between Arctic feedbacks and changes in poleward energy transport. *Geophys. Res. Lett.*, **38**, L17704, https://doi.org/10.1029/2011GL048546.

Kang, S. M., I. M. Held, D. M. Frierson, and M. Zhao, 2008: The response of the ITCZ to extratropical thermal forcing: Idealized slab-ocean experiments with a GCM. *J. Climate*, **21**, 3521–3532, https://doi.org/10.1175/2007JCLI2146.1.

Kay, J., B. Medeiros, Y.-T. Hwang, A. Gettelman, J. Perket, and M. Flanner, 2014: Processes controlling Southern Ocean shortwave climate feedbacks in CESM. *Geophys. Res. Lett.*, **41**, 616–622, https://doi.org/10.1002/2013GL058315.

——, and Coauthors, 2015: The Community Earth System Model (CESM) Large Ensemble project: A community resource for studying climate change in the presence of internal climate variability. *Bull. Amer. Meteor. Soc.*, **96**, 1333–1349, https://doi.org/10.1175/BAMS-D-13-00255.1.

Knutti, R., and G. C. Hegerl, 2008: The equilibrium sensitivity of the Earth's temperature to radiation changes. *Nat. Geosci.*, **1**, 735–743, https://doi.org/10.1038/ngeo337.

——, M. A. Rugenstein, and G. C. Hegerl, 2017: Beyond equilibrium climate sensitivity. *Nat. Geosci.*, **10**, 727–736, https://doi.org/10.1038/ngeo3017.

Koll, D. D., and T. W. Cronin, 2018: Earth's outgoing longwave radiation linear due to H_2O greenhouse effect. *Proc. Natl. Acad. Sci. USA*, **115**, 10293–10298, https://doi.org/10.1073/pnas.1809868115.

Kuhlbrodt, T., and J. Gregory, 2012: Ocean heat uptake and its consequences for the magnitude of sea level rise and climate change. *Geophys. Res. Lett.*, **39**, L18608, https://doi.org/10.1029/2012GL052952.

Li, C., J.-S. von Storch, and J. Marotzke, 2013: Deep-ocean heat uptake and equilibrium climate response. *Climate Dyn.*, **40**, 1071–1086, https://doi.org/10.1007/s00382-012-1350-z.

Lin, Y.-J., Y.-T. Hwang, P. Ceppi, and J. M. Gregory, 2019: Uncertainty in the evolution of climate feedback traced to the strength of the Atlantic Meridional Overturning Circulation. *Geophys. Res. Lett.*, **46**, 12331–12339, https://doi.org/10.1029/2019GL083084.

Liu, W., A. V. Fedorov, S.-P. Xie, and S. Hu, 2020: Climate impacts of a weakened Atlantic Meridional Overturning Circulation in a warming climate. *Sci. Adv.*, **6**, eaaz4876, https://doi.org/10.1126/sciadv.aaz4876.

LoPresti, A., A. Charland, D. Woodard, J. Randerson, N. S. Diffenbaugh, and S. J. Davis, 2015: Rate and velocity of climate change caused by cumulative carbon emissions. *Environ. Res. Lett.*, **10**, 095001, https://doi.org/10.1088/1748-9326/10/9/095001.

Lu, J., G. A. Vecchi, and T. Reichler, 2007: Expansion of the Hadley cell under global warming. *Geophys. Res. Lett.*, **34**, L06805, https://doi.org/10.1029/2006GL028443.

Mahlstein, I., and R. Knutti, 2011: Ocean heat transport as a cause for model uncertainty in projected Arctic warming. *J. Climate*, **24**, 1451–1460, https://doi.org/10.1175/2010JCLI3713.1.

Manabe, S., and R. J. Stouffer, 1980: Sensitivity of a global climate model to an increase of CO_2 concentration in the atmosphere. *J. Geophys. Res.*, **85**, 5529–5554, https://doi.org/10.1029/JC085iC10p05529.

Mertz, O., K. Halsnæs, J. E. Olesen, and K. Rasmussen, 2009: Adaptation to climate change in developing countries. *Environ. Manage.*, **43**, 743–752, https://doi.org/10.1007/s00267-008-9259-3.

Morrison, A. K., S. M. Griffies, M. Winton, W. G. Anderson, and J. L. Sarmiento, 2016: Mechanisms of Southern Ocean heat uptake and transport in a global eddying climate model. *J. Climate*, **29**, 2059–2075, https://doi.org/10.1175/JCLI-D-15-0579.1.

Neale, R., and Coauthors, 2012: Description of the NCAR Community Atmosphere Model (CAM 5.0). NCAR Tech. Note TN-486+STR, 289 pp., www.cesm.ucar.edu/models/cesm1.0/cam/docs/description/cam5_desc.pdf.

Nummelin, A., C. Li, and P. Hezel, 2017: Connecting ocean heat transport changes from the midlatitudes to the Arctic Ocean. *Geophys. Res. Lett.*, **44**, 1899–1908, https://doi.org/10.1002/2016GL071333.

O'Neill, B. C., and Coauthors, 2016: The scenario model intercomparison project (ScenarioMIP) for CMIP6. *Geosci. Model Dev.*, **9**, 3461–3482, https://doi.org/10.5194/gmd-9-3461-2016.

Oleson, K., and Coauthors, 2010: Technical description of version 4.0 of the Community Land Model (CLM). NCAR Tech. Note NCAR/TN-478+STR, 257 pp., https://doi.org/10.5065/D6FB50WZ.

Orlove, B., 2005: Human adaptation to climate change: A review of three historical cases and some general perspectives. *Environ. Sci. Policy*, **8**, 589–600, https://doi.org/10.1016/j.envsci.2005.06.009.

Peixoto, J., and A. Oort, 1992: *Physics of Climate*. American Institute of Physics, 520 pp.

Pendergrass, A. G., A. Conley, and F. M. Vitt, 2018: Surface and top-of-atmosphere radiative feedback kernels for CESM-CAM5. *Earth Syst. Sci. Data*, **10**, 317–324, https://doi.org/10.5194/essd-10-317-2018.

Raper, S. C., J. M. Gregory, and R. J. Stouffer, 2002: The role of climate sensitivity and ocean heat uptake on AOGCM transient temperature response. *J. Climate*, **15**, 124–130, https://doi.org/10.1175/1520-0442(2002)015<0124:TROCSA>2.0.CO;2.

Rencurrel, M. C., and B. E. Rose, 2018: Exploring the climatic response to wide variations in ocean heat transport on an aquaplanet. *J. Climate*, **31**, 6299–6318, https://doi.org/10.1175/JCLI-D-17-0856.1.

Rind, D., and M. Chandler, 1991: Increased ocean heat transports and warmer climate. *J. Geophys. Res.*, **96**, 7437–7461, https://doi.org/10.1029/91JD00009.

Roe, G. H., and M. B. Baker, 2007: Why is climate sensitivity so unpredictable? *Science*, **318**, 629–632, https://doi.org/10.1126/science.1144735.

Rose, B., and D. Ferreira, 2013: Ocean heat transport and water vapor greenhouse in a warm equable climate: A new look at the low gradient paradox. *J. Climate*, **26**, 2117–2136, https://doi.org/10.1175/JCLI-D-11-00547.1.

Rugenstein, M. A., M. Winton, R. J. Stouffer, S. M. Griffies, and R. Hallberg, 2013: Northern high-latitude heat budget decomposition and transient warming. *J. Climate*, **26**, 609–621, https://doi.org/10.1175/JCLI-D-11-00695.1.

——, K. Caldeira, and R. Knutti, 2016: Dependence of global radiative feedbacks on evolving patterns of surface heat fluxes. *Geophys. Res. Lett.*, **43**, 9877–9885, https://doi.org/10.1002/2016GL070907.

Russell, J. L., K. W. Dixon, A. Gnanadesikan, R. J. Stouffer, and J. Toggweiler, 2006: The Southern Hemisphere westerlies in a warming world: Propping open the door to the deep ocean. *J. Climate*, **19**, 6382–6390, https://doi.org/10.1175/JCLI3984.1.

Seeley, J. T., and N. Jeevanjee, 2021: H_2O windows and CO_2 radiator fins: A clear-sky explanation for the peak in equilibrium climate sensitivity. *Geophys. Res. Lett.*, **48**, e2020GL089609, https://doi.org/10.1029/2020GL089609.

Shell, K., J. Kiehl, and C. Shields, 2008: Radiative kernel technique to calculate climate feedbacks in NCAR's Community Atmospheric Model. *J. Climate*, **21**, 2269–2283, https://doi.org/10.1175/2007JCLI2044.1.

Sherwood, S., and Coauthors, 2020: An assessment of Earth's climate sensitivity using multiple lines of evidence. *Rev. Geophys.*, **58**, e2019RG000678, https://doi.org/10.1029/2019RG000678.

Singh, H., P. Rasch, and B. Rose, 2017: Increased ocean heat convergence into the high latitudes with CO_2 doubling enhances polar-amplified warming. *Geophys. Res. Lett*, **44**, 10583–10591, https://doi.org/10.1002/2017GL074561.

——, O. A. Garuba, and P. Rasch, 2018: How asymmetries between Arctic and Antarctic climate sensitivity are modified by the ocean. *Geophys. Res. Lett.*, **45**, 13031–13040, https://doi.org/10.1029/2018GL079023.

Soden, B., I. Held, R. Colman, K. Shell, and J. Kiehl, 2008: Quantifying climate feedbacks using radiative kernels. *J. Climate*, **21**, 3504–3520, https://doi.org/10.1175/2007JCLI2110.1.

Sokolov, A. P., C. E. Forest, and P. H. Stone, 2003: Comparing oceanic heat uptake in AOGCM transient climate change experiments. *J. Climate*, **16**, 1573–1582, https://doi.org/10.1175/1520-0442-16.10.1573.

Stone, P., 1978: Constraints on dynamical transports of energy on a spherical planet. *Dyn. Atmos. Oceans*, **2**, 123–139, https://doi.org/10.1016/0377-0265(78)90006-4.

Stouffer, R. J., J. Russell, and M. J. Spelman, 2006: Importance of oceanic heat uptake in transient climate change. *Geophys. Res. Lett.*, **33**, L17704, https://doi.org/10.1029/2006GL027242.

Sutton, R., and P.-P. Mathieu, 2002: Response of the atmosphere-ocean mixed-layer system to anomalous ocean heat-flux convergence. *Quart. J. Roy. Meteor. Soc.*, **128**, 1259–1275, https://doi.org/10.1256/003590002320373283.

Trossman, D., J. Palter, T. Merlis, Y. Huang, and Y. Xia, 2016: Large-scale ocean circulation–cloud interactions reduce the pace of transient climate change. *Geophys. Res. Lett.*, **43**, 3935–3943, https://doi.org/10.1002/2016GL067931.

Vellinga, M., and R. A. Wood, 2002: Global climatic impacts of a collapse of the Atlantic thermohaline circulation. *Climatic Change*, **54**, 251–267, https://doi.org/10.1023/A:1016168827653.

——, and P. Wu, 2008: Relations between northward ocean and atmosphere energy transports in a coupled climate model. *J. Climate*, **21**, 561–575, https://doi.org/10.1175/2007JCLI1754.1.

Weijer, W., W. Cheng, O. A. Garuba, A. Hu, and B. Nadiga, 2020: CMIP6 models predict significant 21st century decline of the Atlantic Meridional Overturning Circulation. *Geophys. Res. Lett.*, **47**, e2019GL086075, https://doi.org/10.1029/2019GL086075.

Wilson, C., and J. Mitchell, 1987: A doubled CO_2 climate sensitivity experiment with a global climate model including a simple ocean. *J. Geophys. Res.*, **92**, 13 315–13 343, https://doi.org/10.1029/JD092iD11p13315.

Winton, M., 2003: On the climatic impact of ocean circulation. *J. Climate*, **16**, 2875–2889, https://doi.org/10.1175/1520-0442(2003)016<2875:OTCIOO>2.0.CO;2.

Xie, P., and G. K. Vallis, 2012: The passive and active nature of ocean heat uptake in idealized climate change experiments. *Climate Dyn.*, **38**, 667–684, https://doi.org/10.1007/s00382-011-1063-8.

Zelinka, M., and D. Hartmann, 2012: Climate feedbacks and their implications for poleward energy flux changes in a warming climate. *J. Climate*, **25**, 608–624, https://doi.org/10.1175/JCLI-D-11-00096.1.

——, S. A. Klein, and D. L. Hartmann, 2012: Computing and partitioning cloud feedbacks using cloud property histograms. Part I: Cloud radiative kernels. *J. Climate*, **25**, 3715–3735, https://doi.org/10.1175/JCLI-D-11-00248.1.